



# *Genesis and variation spatial of Podzol in depressions of the Barreiras formation, northeastern Espírito Santo State, Brazil, and its implications for Quaternary climate change*

Article

Accepted Version

Creative Commons: Attribution-Noncommercial-No Derivative Works 4.0

Schiavo, J. A., Pessenda, L. C. R., Buso Junior, A. A., Calegari, M. R., Fornari, M., Secretti, M. L., Pereira, M. G. and Mayle, F. E. (2020) Genesis and variation spatial of Podzol in depressions of the Barreiras formation, northeastern Espírito Santo State, Brazil, and its implications for Quaternary climate change. *Journal of South American Earth Sciences*, 98.

102435. ISSN 0895-9811 doi:

<https://doi.org/10.1016/j.jsames.2019.102435> Available at

<http://centaur.reading.ac.uk/87432/>

It is advisable to refer to the publisher's version if you intend to cite from the work. See [Guidance on citing](#).

To link to this article DOI: <http://dx.doi.org/10.1016/j.jsames.2019.102435>

Publisher: Elsevier

All outputs in CentAUR are protected by Intellectual Property Rights law, including copyright law. Copyright and IPR is retained by the creators or other copyright holders. Terms and conditions for use of this material are defined in the [End User Agreement](#).

[www.reading.ac.uk/centaur](http://www.reading.ac.uk/centaur)

## **CentAUR**

Central Archive at the University of Reading

Reading's research outputs online

1 **Genesis and variation spatial of Podzol in depressions of the Barreiras Formation,**  
2 **northeastern Espírito Santo State, Brazil, and its implications for Quaternary climate**  
3 **change.**

4 Jolimar Antonio Schiavo<sup>a</sup>, Luiz Carlos Ruiz Pessenda<sup>b</sup>, Antonio Alvaro Buso Júnior<sup>b</sup>, Marcia  
5 Regina Calegari<sup>c</sup>, Mileni Fornari<sup>b</sup>, Mateus Luiz Secretti<sup>a</sup>; Marcos Gervasio Pereira<sup>d</sup>; Frank  
6 Edward Mayle<sup>e</sup>

7 <sup>a</sup>Universidade Estadual de Mato Grosso do Sul, Unidade Universitária de Aquidauana,  
8 Rodovia Aquidauana, km 12, Aquidauana, Mato Grosso do Sul, Brazil.

9 <sup>b</sup>Universidade de São Paulo, Laboratório de <sup>14</sup>C, Avenida Centenário 303, 13400-970,  
10 Piracicaba, São Paulo, Brazil.

11 <sup>c</sup>Universidade Estadual do Oeste do Paraná, Campus Marechal Cândido Rondon, Colegiado  
12 de Geografia, Rua Pernambuco, 1777, CX Postal 91, CEP:85970-020, Mal. Cd Rondon,  
13 Paraná, Brazil.

14 <sup>d</sup>Universidade Federal Rural do Rio de Janeiro, Instituto de Agronomia, Departamento de  
15 Solos, BR-465, Seropédica, Rio de Janeiro, Brazil.

16 <sup>e</sup>University of Reading, Centre for Past Climate Change and Department of Geography &  
17 Environmental Science, Reading RG6 6DW, Berkshire, UK.

18 **ABSTRACT.** Variations in relief associated with pedogenetic processes promote  
19 different intensities in weathering of sediments of the Barreiras Formation and may thus lead  
20 to the formation of different soil types, like Podzols, Acrisols and Ferralsols. The Podzols of  
21 tropical regions contain important information on climate and vegetation changes that  
22 occurred mainly in late Pleistocene and Holocene; however few studied, regarding their  
23 spatial variation, that can be investigated through ground penetrating radar (GPR). The aim  
24 was to study morphological, physical, chemical, stable C isotopic properties and spatial  
25 distribution of soils within depressions of the Barreiras Formation and characterize the <sup>14</sup>C  
26 chronology of two Podzols and their B spodic horizons, along a transect grassland to forest in  
27 northeastern Espírito Santo State, Brazil. The profiles encompass a sequence of A-E-Bhm  
28 horizons, except for P3 and P6 with histic H and A-Bt, respectively. The GPR images showed  
29 patterns corresponding to these soil horizons, and the GPR data reveal the presence of

30 diagnostic subsurface horizons characteristic of spodic horizons with cemented layers. The  
31 influence of relief factors and original materials was observed, associated with ferrollysis and  
32 podzolisation as main actors in the genesis of soils studied. The monomorphic organic matter  
33 filling the voids evidences the processes of immobilization, illuviation and precipitation, with  
34 the genesis of the spodic horizon. The Podzols profiles of Pleistocene organic matter ages  
35 accumulated compounds of C<sub>3</sub> plants from the vegetation cover in the B spodic horizons of  
36 the profiles P4 and P1, since at least 14,251 and 38,890 cal BP, respectively, suggesting the  
37 dominance of a humid climate at least during the studied period in the region.

38 **Keywords:** Ground penetrating radar, Organic matter, Stable carbon isotopes, <sup>14</sup>C dating,  
39 Micromorphology, Podzolisation.

## 40 1. Introduction

41 The north and northeastern regions of Espírito Santo State, Brazil, encompass the  
42 Tabuleiros Costeiros (coastal plains) geomorphological unit, which comprises sandy-clayey  
43 Tertiary deposits of the Barreiras Group. In this coastal plain, there are gentle depressions,  
44 which favor the lateral flow of water with installation of water table, forming types of soils  
45 different from those of the higher parts of the landscape (Pessenda et al., 2015; Calegari et al.,  
46 2017).

47 Ferralsols and Acrisols are predominant soils and occupy the highest parts of the  
48 landscape of this region and have been well studied (Moreau et al., 2006; Corrêa et al., 2008;  
49 Lima Neto et al., 2009; Dantas et al., 2014), and are characterized by sandy loam to clay  
50 texture, yellowish tones, low nutrient availability and cation exchange capacity, exchangeable  
51 aluminum and aluminum saturation, and kaolinite mineralogy (Lima Neto et al., 2009). The  
52 lower parts of the landscape are associated with sandy soils like Arenosols and Podzols. In the  
53 coastal plains, the vegetation shows different physiognomies associated with markedly  
54 different soil types, i.e., Ferralsols and Acrisols are associated with Lowland Tropical

55 Rainforest, while the Arenosols and Podzols are associated with the grasslands (Saporetto-  
56 Junior et al., 2012).

57 The Podzols have important environmental functions such as being a filter for  
58 pollutants and a sink for atmospheric carbon (Sauer et al., 2007; Montes et al., 2011; Lopes-  
59 Mazzetto et al., 2018), as well as representing areas with large numbers of endemic and  
60 niches specific species being designated as conservation areas (Buso Júnior et al., 2013,  
61 Mendonça et al., 2015).

62 Among the various theories proposed to explain the formation of Podzols (Anderson et  
63 al., 1982; Buurman and Jongmans, 2005; DeConinck, 1980; Lundstrom et al., 2000a), the  
64 complexation and transport of dissolved organic matter (DOM) with Fe and Al play an  
65 important role in the formation of the B spodic horizon. Typically, the B spodic horizon  
66 shows colors ranging from black to reddish brown, enriched by organic matter, Al and  
67 sometimes Fe.

68 The natural drainage conditions influence the formation of Podzols, mainly in the  
69 morphology and distinction of horizons, in the accumulation and stabilization of organic  
70 matter and Fe in the B spodic horizon. The presence or absence of Fe can be used as an  
71 indicator of drainage conditions. Poorly drained Podzols have lost all Fe due to reduction and  
72 lateral removal, while in well-drained podzols Fe is still present, and intermediate drainage  
73 conditions are recognised by Fe mottles (Buurman, 1984; DeConinck et al., 1974). In addition  
74 to Fe, drainage conditions can cause variations in the morphology of Podzols as thickness of  
75 the B horizon and the shape of the EB transition, i.e. those poorly drained have flat EB  
76 transition caused by the highest groundwater level; while the well-drained have a thin  
77 undulating Bh horizon, dependent on the vertical movement of percolated water (Buurman et  
78 al., 2005, 2013; Lopes-Mazzetto et al., 2018; Kaczorek et al., 2004; Schwartz, 1988). In  
79 poorly drained podzols, the B horizon is water-saturated during large part of the year, and the

80 organic matter is predominantly DOM derived. In well-drained podzols, the B horizon may  
81 have a contribution from in situ root materials and the DOM has a very local source due to  
82 vertical movement of percolating water (Lopes-Mazzetto et al., 2018). More detailed studies  
83 of organic matter such as determination of the elemental composition by pyrolysis (Lopes-  
84 Mazzetto et al., 2018),  $^{12}\text{C}$  and  $^{13}\text{C}$  isotopic variation,  $^{14}\text{C}$  dating (Horbe et al., 2004) and  
85 Spodic B horizon micromorphology (Bardy et al., 2008; Coelho et al., 2012) may contribute  
86 to inferring the genesis of Podzols.

87         The podzols of tropical environments, such as those of coastal plain in Brazil, may be  
88 much older and consequently with greater variations of climate and vegetation (Boski et al.,  
89 2015; Martinez et al., 2018), when compared to Podzols of boreal and temperate areas with  
90 Holocene age with moderate variations in the climate.

91 In Brazil, detailed studies of the classification and genesis of Podzols have been made in  
92 individual profiles (Mafra et al., 2002; Coelho et al., 2010b; Coelho et al., 2010c; Oliveira et  
93 al., 2010; Schiavo et al., 2012; Carvalho et al., 2013), but little is known about the spatial  
94 variation of the podzolisation process as a function of climate and vegetation.

95         Vale Nature Reserve (VNR) is a 28,000-hectare area of protected vegetation, located  
96 in the northeastern Espirito Santo State, in the municipality of Linhares, Brazil. The  
97 vegetation shows different physiognomies associated with markedly different soil types. Soil  
98 variations across the landscape can be better understood in the context of micro-relief and  
99 associated variations in vegetation type. The Tabuleiros forest (Lowland Tropical Rainforest)  
100 is the dominant matrix, occurring in the higher parts of the landscape, being associated with  
101 Ferralsols and Acrisols (Moreau et al., 2006; Corrêa et al., 2008; Lima Neto et al., 2009; Silva  
102 et al., 2013; Dantas et al., 2014). Mussununga vegetation occurs interspersed with the  
103 Tabuleiros forest and varies from grasslands (campos nativos) to wooded savannah and  
104 woodland (Saporetto-Junior et al., 2012) and it is associated with sandy soils such as

105 Arenosols and Podzols (Pessenda et al., 2015; Calegari et al., 2017; Buso Júnior et al., 2019).  
106 In this region, these authors verified using distinct proxies (pollen,  $\delta^{13}\text{C}$ ,  $\delta^{15}\text{N}$ ,  $^{14}\text{C}$  dating and  
107 phytoliths) that the Podzols genesis is related to changes in vegetation and climate, occurring  
108 between the Holocene and late Pleistocene.

109 In this environment, the ground penetrating radar (GPR) is a tool that can contribute to  
110 the understanding of the spatial variation and arrangement (thickness, depth and transition) of  
111 the horizons of Podzols. According to the principle of GPR, the morphological differentiation  
112 between the horizons of the Podzols can be detected by the emission of different  
113 electromagnetic pulses (Ucha et al., 2010), and consequently, it can be inferred in the spatial  
114 distribution of these horizons.

115 The aim of the present study is to characterize the morphological, physical and  
116 chemical properties of soils (Podzol), associated with GPR data and stable C isotopes of the  
117 soil profile, across the ecotone between native grassland and Tabuleiro forest in northeastern  
118 Espírito Santo State, Brazil, in order to understand the genesis and spatial distribution of the B  
119 spodic horizon and its relation to vegetation and soil properties.

## 120 **2. Study site**

121 The study area is located in the Vale Nature Reserve (VNR), northeastern of the  
122 Espírito Santo State, Brazil. The VRN is a protected area within the natural range of the  
123 lowland Atlantic Forest, and it is one of the most important areas for biodiversity  
124 conservation (Ministério do Meio Ambiente, 2000).

125 The geological landscape is characterized by highland areas with Precambrian rocks,  
126 offering an uneven relief occupied by Atlantic Forest, and a system of dendritic rivers. The  
127 Neogene plateau to the east of the relief, locally called Tabuleiros Costeiros, is formed by  
128 continental deposits of the Barreiras Formation (Tertiary period), a flat terrain with a  
129 corrugated slope towards the sea. The Tabuleiros comprises marine, fluvial-marine, lagoon

130 and eolian sediments accumulated during the Quaternary. The Tabuleiros evolution was  
131 strongly controlled by relative sea-level changes, fluvial sedimentation, long shore drift, and  
132 changes in atmospheric circulation (Martin et al., 1993).

### 133 **3. Material and methods**

134 The soil sampling was carried out in the VNR (19°11'58" S and 40°05'22" W. Fig. 1).  
135 The climate in the region is warm and humid, tropical type (Aw), with a rainy season in the  
136 austral summer and dry winter, mean annual precipitation of 1215 mm, mean annual  
137 temperature of 23.3 °C (Buso Junior et al. 2013). In the area of the VNR, it is possible to  
138 distinguish (with a resolution of ~5.0 meters) distinct vegetation-soil relationships in circular  
139 areas of grasslands within Tabuleiro forest, with transitional shrub vegetation.

140 Six trenches were dug within two study areas spanning the center of the grassland to  
141 the Tabuleiro forest: transect 1 – profile P1: 19° 09' 11.30" S 40° 03'55.40" W (grassland  
142 mussununga), P2: 19° 09'16.20" S 40° 03' 54.80" W (shrubland mussununga), P3: 19°  
143 09'17.16" S 40° 03'55.20" W (woodland mussununga); transect 2 – profile P4: 19°12'47.00"  
144 S 39° 57'52.00" W (grassland mussununga), P5: 19°12'36.10" S 39° 57'40.80" W (shrubland  
145 mussununga) and P6: 19° 12'35.34" S 39° 57'36.30" W (woodland mussununga). Inside the  
146 trenches the profiles were morphologically described based on Santos et al. (2015), and  
147 samples collected from all horizons. Disturbed soil samples were air-dried, ground and sieved  
148 (fraction < 2 mm) to be used for physical and chemical analyses as described in Teixeira et al.  
149 (2017). The particle size was determined by the pipette method, using sodium hydroxide 0.1  
150 mol L<sup>-1</sup> as dispersant.

151 To determine and map the soil horizons and assess spatial variations in soil properties,  
152 ground-penetrating radar (GPR) was used along 15 km, with transects across a representative  
153 soil area using the TerraSIR Subsurface Interface Radar (SIR) System-3000 (Geophysical  
154 Survey Systems, Inc., Salem, New Hampshire) with 200 MHz antenna (Fig. 1). The 200-MHz



155 frequency was chosen after in situ testing with a series of antenna frequencies (70 MHz, 400  
156 MHz, 270 MHz and 200 MHz). The 200 MHz frequency provided the optimal balance of  
157 image quality, detection depth, and the convenience of operation in the area with both  
158 grassland and Tabuleiro forest. Traces along the GPR transects were adjusted vertically for  
159 variations in topography, using a real time kinematic global positioning system. Data  
160 processing included applying a zero time adjustment to find true ground surface reflection,  
161 same gain factor, dewow filter, a tapered bandpass filter (20–40–300–600 MHz) and an  
162 automatic gain control (AGC), using the RADAN for Windows™ software program (version  
163 7, GSSI).

164 The exchangeable cations  $\text{Ca}^{2+}$ ,  $\text{Mg}^{2+}$  and  $\text{Al}^{3+}$  were extracted with  $1\text{ mol L}^{-1}$  KCl  
165 solution, the H+Al with a  $0.5\text{ mol L}^{-1}$  calcium acetate solution with pH 7.0. For the extraction  
166 of P,  $\text{Na}^{+}$  and  $\text{K}^{+}$  the solution of  $\text{H}_2\text{SO}_4\ 0.0125\text{ mol L}^{-1} + \text{HCl}\ 0.05\text{ mol L}^{-1}$  was used. The  
167 levels of  $\text{Ca}^{2+}$  and  $\text{Mg}^{2+}$  were determined by titrations with  $0.0125\text{ mol L}^{-1}$  EDTA solution;  
168  $\text{Na}^{+}$  and K by flame photometry; P by colorimetry; and  $\text{Al}^{3+}$  and H+ Al, by titrations with  
169  $\text{NaOH}\ 0.025\text{ mol L}^{-1}$ . The pH in water and KCl (weight 1:2.5) was determined by means of a  
170 potentiometer. The content of total organic carbon (TOC) was determined according to  
171 Yeomans and Bremner (1988). From these results, the following were calculated: the  
172 saturation by aluminum (m); the SB value (sum of exchangeable bases); T value (CTC of the  
173 ground) and V value. All the above procedures were carried out according to Teixeira et al.  
174 (2017).

175 The forms of Fe and Al, in their varying degrees of crystallinity, were evaluated by the  
176 use of sodium dithionite–citrate–bicarbonate (DCB) (Mehra and Jackson, 1960), and of acid  
177 ammonium oxalate (Ox), (McKeague and Day, 1966), with determination of extracts by  
178 atomic absorption spectrometry.

179           The profiles P1 and P4, horizons Bhx1 (1.49-1.60 m) and Bhm1/Bhm2 (0.91-1.11 m)  
180 respectively, were selected for  $^{14}\text{C}$  dating. These soil samples were treated according to  
181 Pessenda et al. (1996) for humin extraction. Treatments included the removal of modern roots  
182 fragments by handpicking, followed by the removal of fulvic and humic acids. The samples  
183 were combusted at the  $^{14}\text{C}$  Laboratory and the purified  $\text{CO}_2$  was sent to the LACUFF  
184 Laboratory, Brazil for accelerator mass spectrometry (AMS) dating (Macario et al., 2013).  
185 Ages are expressed as years before present (BP) and calibrated ages (cal. BP,  $2\sigma$ ), according  
186 to the SHCal13 curve (Hogg et al., 2013), using the software CALIB Rev 7.0.4 (Stuiver and  
187 Reimer, 1993) for  $^{14}\text{C}$  age calibration.

188           In addition, in the profiles P1 and P4 (native grassland) soil samples were collected  
189 each 10 cm for analysis of carbon stable isotopes ( $\delta^{13}\text{C}$ ). The profiles P1 and P4 were  
190 collected up to 1.8 m and 3.70 m, respectively. Modern root fragments were manually  
191 removed from soil samples selected for C analyses and sieved (350  $\mu\text{m}$ ) with distilled water to  
192 remove coarse sand grains. All samples were dried at 50  $^\circ\text{C}$ . Analyses were carried out at the  
193 Stable Isotope Laboratory (CENA/USP) using an elemental analyzer attached to an ANCA  
194 SL 2020 mass spectrometer. Stable isotopes ( $\delta^{13}\text{C}$ ) were measured with respect to VPDB as  
195 standard and are expressed as *per mil* (‰) with a standard deviation of 0.2‰.

196           The natural oriented samples taken for micromorphological analyses were collected in  
197 horizon B spodic of the profiles P2 and P5 (0.69-0.81 m and 0.87-0.98 m, respectively),  
198 impregnated with a mixture of Polilyte polyester resin, styrene monomer, and fluorescent  
199 pigment, using Butanox as a catalyst (de Castro et al., 2003), to prepare 30- $\mu\text{m}$  fine sections.  
200 The sections were observed using a polarizing optical microscopic (Carl Zeiss, Lab.A1 Axio,  
201 Germany) and binocular magnifier (Carl Zeiss, 444036-9010, Germany), both under normal  
202 and polarized light. Photomicrographs were obtained using a photomicroscopic camera (Carl

203 Zeiss, Axiocam 305 color, Germany). The micromorphological descriptions followed the  
204 criteria and terminologies proposed by Bullock et al. (1985) and Stoops (2003).

205 From the morphological descriptions and analytical data (chemical and physical), soils  
206 were classified according to the World Reference Base for Soil Resources (IUSS Working  
207 Group WRB, 2015), in Podzols (profiles P1, P2, P3, P4 and P5) and Acrisols (P6).

### 208 **3. Results and Discussion**

#### 209 **3.1. Morphological and physical attributes**

210 Soils described in both transects showed differences in terms of color, structure,  
211 consistence, soil thickness, transition between horizons and physical attributes (Table 1).

212 Except for profile P6 that has a sequence of A-Btg horizons, the other profiles showed  
213 a spodic A-E-B sequence. In these profiles, underlying the E albic horizon, the spodic B  
214 horizon appeared cemented in varying degrees, with a massive structure, characteristic of  
215 ortstein, occurring with different thicknesses and at different depths (Fig. 2). Farmer et al.  
216 (1983) indicate that this cementation occurs between the grains of quartz and organic  
217 compounds. In profiles P1, P2 and P3 the duric horizon occurs below the spodic B horizon  
218 (Santos et al., 2015), a feature also observed by Oliveira et al. (2010) and Carvalho et al.  
219 (2013) in Podzols of the Barreiras Formation in southern Bahia and Paraíba, respectively,  
220 northeastern Brazil.

221 This interpretation is also supported by GPR data (Fig. 2). The GPR1 line (Fig. 2) in  
222 the transect 1 (Fig. 1) reaches up to ~2.0 m thick and shows a distinct interface between the  
223 two contrasting materials with a lateral extension of several hundreds of meters (Fig. 2). At  
224 the top of the radargram, there are continuous sand medium amplitude and sub-horizontal  
225 reflections that extend from the top of the record to 1.5 m. These reflections could be related  
226 to the A and E horizon that resulted in a lower contrast in soil electrical properties and a

227 weaker GPR reflection, probably due to the process of the progressive illuviated silicate clays,  
228 with migration of clay-humus complexes to the underlying horizons. These conditions favor  
229 the infiltration and drainage of rainwater for the B spodic horizon (Doolittle and Collins,  
230 1995; Burgoa et al., 1991). On the radar record, the lower part of the A-E horizon is  
231 characterized by a continuous strong reflection, showing a wavy or irregular geometry. This  
232 reflection corresponds approximately to the top of the B spodic (1.5 m depth), i.e., below of  
233 the spodic horizon, soil that contains silt or loamy particle-size classes with significant levels  
234 of moisture and organic carbon that can be related to genesis of duric horizon. The processes  
235 associated with duric horizon formation result in hydro-consolidation that causes close  
236 packing of grains and reduces porosity (Bockheim and Hartemink, 2013). The latter generates  
237 a high radar signal associated with the presence of diagnostic subsurface horizons,  
238 represented by a spodic horizon. Duric horizon has higher bulk densities and is less permeable  
239 than overlying or underlying horizons (Doolittle et al., 2005), which can be significantly  
240 attenuated by radar energy below the top of spodic horizons and no clear reflections were  
241 detectable in the lower part of the radar record (Fig. 2; GPR1).

242         The GPR2 line (Fig. 2) obtained between P5 and P6 trenches (Fig. 1) reaches a depth  
243 of 3 m in the soil horizons, below which are weathered deposits of the Barreiras Formation  
244 which extend to > 4 m. The high-amplitude interval lies around 1 m and shows a continuous  
245 reflecting horizon, that can be coincident with the spodic horizon in P5 and/or Btg1 in P6. The  
246 top of the profile (Fig. 2) is dominated by discontinuous low amplitude, parallel to sub-  
247 horizontal reflections which appear to be related to the A horizon which is affected by water  
248 infiltration, plant root penetration and undecomposed organic matter. These conditions favor  
249 the occurrence of water in the near-surface layer (Mendonça et al., 2015), which can reflect a  
250 discontinuity in the GPR signal at the top.

251           On the radargram GPR3 (Fig. 2) recorded at transect 2 (Fig. 1), the soil profile reaches  
252 4 m, with great spatial variability in thickness (up to 6 m) and consists of three different  
253 reflection patterns. The upper part, extending to 1.5 m, contains near horizontal internal  
254 reflections with a strong amplitude signal and extends along the whole GPR profile. These  
255 stronger reflections signify a continuous A-E horizon and are interpreted as layers that contain  
256 significant accumulations of silicate clay, organic matter and Fe and Al. Below this section,  
257 down to 1 m, internal reflections change from subparallel to wavy with a concave shape and  
258 show a lateral extension of up to hundreds of meters with reflectors more segmented. While  
259 the highest amplitudes are restricted to reflections in the depth range of 0.5 to 1 m, reflections  
260 beneath were attenuated rapidly and are of low to very low amplitude (Fig. 2). These  
261 reflectors are attributed to cemented spodic horizons and can be associated with the presence  
262 of ortstein traced laterally on GPR lines. Cemented horizons are more compacted, with fewer  
263 pores and differences in textural properties (Doolittle and Butnor, 2009; Afshar et al., 2017)  
264 when compared to the overlapping layers and can generate high amplitude, and greater  
265 attenuation of the GPR signal. As reported by Mokma et al (1990), the increased signal  
266 reflections from the spodic horizon can produce high amplitude reflections that are associated  
267 with the presence of ortstein. The lowermost boundaries are imaged as high-amplitude and  
268 contain subparallel to concave reflections and, lateral discontinuity, from which noises occur.  
269 This unconformity at a depth of around 4-5 m forms the lower boundary of the soil profile,  
270 which can be attributed to weathered bedrock surfaces of the Barreiras Formation in situ.

271           The GPR data (Fig. 2) show that the top of the spodic horizons ranges in depth from  
272 about 0.6 to 2 m and developed in response to the process of reworking of weathered deposits  
273 of the Barreiras Formation, from which the radar energy was significantly attenuated, and no  
274 clear reflections are detectable. As reported by Doolittle and Butnor (2009), because of

275 differences in their bulk density and water retention capacity, spodic horizons are detectable  
276 with GPR.

277 Spodic horizons of profiles P1, P2, P3, P4 and P5 have a 10YR matrix with dark and  
278 gray hues (low value and chroma), mainly due to the high content of organic matter, while in  
279 albic E horizons, due to the multiple pedogenetic processes of translocation, whitish colors  
280 were observed (high value). The presence of the E horizon is an indication of the pedogenetic  
281 process of leucinization which creates a lighter coloured horizon (Kämpf and Curi, 2012). In  
282 general, these profiles have a structure ranging from granular to simple grains in A and E  
283 horizons, and massive in the spodic B. Furthermore, the consistency of the surface horizons  
284 was loose, while consistency of the spodic B horizons ranged from hard to extremely hard. In  
285 general, all horizons had a wet non-plastic and non-sticky consistency. This characteristics of  
286 soil consistency is a result of the coarse grain size in the horizons. Fine sand is predominant in  
287 the profiles. The textural class ranges between sand, loamy sand, sandy loam and sandy clay  
288 loam.

289 The differences in the depths of spodic B horizons, observed in the two areas studied,  
290 is related to the oscillation of the water table, which is influenced by the altitude and shape of  
291 the relief (Santos et al., 2015; Coelho et al., 2010c). The GPR transect fluctuations of the  
292 reflected signal in the radargram (Fig. 2) confirmed the variation in the depth of the spodic  
293 horizon in the study areas. The largest dimensions occurred where the profile P1 is located,  
294 the level of the water table is far below the surface ( $> 1.0$  m), and consequently, the top of the  
295 spodic B horizon is formed from 1.43 m depth, and the albic E horizon is  $\sim 1.07$  m thick. On  
296 the other hand, for soils in micro-depressions, the water table occurs closer to the surface  
297 ( $< 1.0$  m) for most of the year. In these cases, as noted in the profiles P2 and P5, the albic E  
298 horizons range in thickness from 0.16 to 0.36 m and the spodic B are formed near the surface  
299 (0.60 m).

300 The P6 profile has a 10YR hue in the superficial horizons, with low chroma and value,  
301 with colors ranging from dark gray brown to black. In sub-surface horizons the 2.5 Y hue is  
302 predominant, with colors ranging from light grayish brown to light yellow brown. In this  
303 profile, in superficial horizons, a granular-type structure occurs and in the sub superficial  
304 blocks, it was sub angular. A clay increment was observed with depth, with a textural gradient  
305 of 1.8 associated with the textural class clay and clay loam. The increment of clay causes the  
306 texture to be sticky and plastic when humid in the subsurface horizons of profile P6. In the  
307 GPR2 line the high reflection amplitudes up to 1m indicate abrupt changes in wave energy  
308 which, can be attributed to an alternation in grain-size with the clay-rich B horizon.

309 It should be noted that in the subsurface horizons of the profiles, at a depth varying  
310 from 124 cm in profile P5 to 182 cm in P6, all material had a similar grain size, possibly as a  
311 result of the weathering in the Barreiras Formation.

### 312 **3.2. Chemical attributes**

313 The highest levels of TOC were observed in the surface horizons (horizon A and H) of  
314 all profiles, as well as in subsurface spodic B horizons of the profiles P1, P2, P3, P4 and P5,  
315 which is characteristic of the process of translocation of organic matter (Table 2). Depending  
316 on the sandy nature, the high levels of TOC influenced the sorption complex of the soils  
317 under study.

318 The pH values in water ranged from 3.8 on the Bhm2 horizon of profile P4, to 6.2 in  
319 the Bhx1 of profile P3, classified as extremely to moderately acidic, respectively (Santos et  
320 al., 2018). This pattern of high acidity of Podzols is related to the high values of  $H^+$  and  $Al^{3+}$   
321 present in the organic matter, mainly in the surface and subsurface spodic B horizons,  
322 corroborating other studies in sandbank areas (Gomes et al., 2007; Coelho et al., 2010c) and  
323 in the Barreiras Formation (Oliveira et al., 2010; Mafra et al., 2002, Silva et al., 2013;  
324 Carvalho et al., 2013).

325           The highest levels of P occurred in subsurface horizons, with maximum values of 117  
326 mg kg<sup>-1</sup>, in the Bx2 horizon of the P2. Oliveira et al. (2010) observed high P content in  
327 Podzols of sandbank areas in the Barreiras Formation and that P is complexed with organic  
328 matter, being translocated in the profile and piling up on the spodic B due to the sandy soil  
329 texture. In addition, the reduction of crystallinity of iron oxides (Silva et al., 2013) by organic  
330 acids also explains the accumulation of P on the spodic B horizon.

331           In general the values of the exchangeable cations were low, K<sup>+</sup> was not detectable, and  
332 Na<sup>+</sup>, Ca<sup>2+</sup> and Mg<sup>2+</sup> ranged from 0 to 0.38, 0 to 2.1 and 0.1 to 2.9 cmol<sub>c</sub> kg<sup>-1</sup>, respectively,  
333 reflecting the low values of sum and bases saturation, characteristic of the Podzols category  
334 (Dias et al., 2003; Oliveira et al., 2010; Coelho et al., 2010 c; Mafra et al., 2002; Carvalho et  
335 al., 2013; Silva et al., 2013).

336           As with the total carbon content, the surface and B spodic horizons presented the  
337 highest levels of Al<sup>3+</sup>, H<sup>+</sup> and H + Al, suggesting that Al complex with organic material is  
338 largely responsible for the genesis of the spodic B horizon (Van Breemen and Buurman,  
339 1998). However, microbial degradation of organic compounds of the spodic B horizon can  
340 promote the release and increase of exchangeable Al, as noted by Oliveira et al. (2010), in  
341 agreement with the data of this study. Several studies have found high levels of Al<sup>3+</sup> in the  
342 spodic B horizon in different Podzol formation environments, such as sandbank areas (Coelho  
343 et al., 2010 c), the Barreiras Formation (Correa et al., 2008; Oliveira et al., 2010) and in the  
344 North region (Mafra et al., 2002).

345           The forms of crystallinity of Fe and Al varied depending on the soils, as well as on  
346 depth in the profiles (Table 3). In the profiles P1, P2, P3, P4 and P5, besides the exchangeable  
347 Al, the Al content in oxalate extracts and DCB showed an accumulation of that element in  
348 spodic B horizons. The extracts of Fe oxalate and DCB showed low levels and did not vary  
349 with soil depth, suggesting greater participation of the Al complexed to the organic acids in



350 the process of podzolisation, during the genesis of the spodic horizon (Coelho et al., 2010c;  
351 Oliveira et al., 2010). The Al/Fe ratios are high in both extracts, highlighting the relatively  
352 greater contribution of Al compared to Fe in the formation of the spodic B horizon. In  
353 addition, the  $Al_{ox}/Al_{DCB}$  ratio in subsurface horizons of all profiles studied was greater than  
354 the unit, indicative of the predominance of distinct forms of this element of lower  
355 crystallinity.

356 This pattern occurs as a result of the high levels of Al of the Barreiras Formation, as  
357 well as the hardening of the spodic horizon and the presence of duric horizon, that create an  
358 environment of water saturation, reducing and removing Fe from the system (Anderson et al.,  
359 1982; Corrêa et al., 2008; Coelho et al., 2010c; Oliveira et al., 2010; Carvalho et al., 2013;  
360 Silva et al., 2013). This process is intensified in soils of sandy texture, similar to those  
361 observed in the study area.

362 In the P6 profile, the Al levels were higher compared to Fe, both in DCB extracts and  
363 in oxalate, but without accumulation in specific horizons. The water table near the surface  
364 (~.1 m) provided a sharp build-up of organic matter and formation of subsurface Btg horizon  
365 with reductomorphic characteristics, with grayish colors typical of a reducing environment  
366 and removal of Fe (Santos et al., 2018), while Al was connected to the organic matter.

### 367 **3.3. $\delta^{13}C$ and $^{14}C$ ages of soil organic matter**

368 The  $\delta^{13}C$  of soil organic matter varied from -28.89 ‰ to -27.57 ‰ in profile P1, and  
369 -28.42 ‰ to -25.28 ‰ in the profile P4 (Fig. 3), characterizing the dominance of  $C_3$  plants in  
370 both sites. These values are similar to those found in the modern dominant plants' species in  
371 the areas of profiles P1 (*Renvoizea trinii*) and P4 (*R. trinni* and *Lagenocarpus rigidus*), which  
372 are  $C_3$  plants and present  $\delta^{13}C$  of -28.9 ‰ and -28.4 ‰, respectively (Buso Junior et al.,  
373 2013). Enriched values of  $\delta^{13}C$  observed in the B spodic horizons (P1 = -27.57‰; P4 =  
374 -25.28‰) may be related to the isotopic fractionation resulted from organic matter

375 decomposition (Macko and Estep, 1984) and do not reflect changes in relative abundance of  
376 C<sub>3</sub> and C<sub>4</sub> plants.

377 The <sup>14</sup>C ages obtained from the humin in the B spodic horizons varied from 38,890 to  
378 14,251 cal BP in profiles P1 and P4, respectively. Then, <sup>14</sup>C ages and δ<sup>13</sup>C values indicate that  
379 C<sub>3</sub> plants dominate the vegetation of the studied sites at least since the late Pleistocene.

380 Considering the organic matter in the B spodic horizon as a mixture of humin fractions  
381 with different ages, the <sup>14</sup>C ages obtained may reflect the minimum age, an aspect also  
382 recorded by Perrin et al. (1964). They considered that in biologically inert B spodic horizons  
383 of tropical oligotrophic Podzols, with low organic matter cycling, the <sup>14</sup>C ages would reflect  
384 the minimum age of formation of these horizons. Buurman and Jongmans (2005) argued that  
385 oligotrophic Podzols in the tropical region, with reduced biologic activity, present longer  
386 residence time of the organic matter in the B spodic horizon. Consequently, the difference in  
387 the ages between P1 and P4 profiles would indicate differences in the time of formation of the  
388 Podzols and/or in the vegetation covering in both sites. A similar situation was observed by  
389 Schwartz (1988) in Podzols in Congo, with ages varying from ~40,000 to 10,000 years BP.

390 In relation to environmental conditions that may lead to Podzol formation, Schwartz  
391 (1988) related the ages of formation of spodic horizons with the time intervals of more humid  
392 climates in Congo. Dubroeuq and Volkoff (1998) suggested that the process of Podzols  
393 formation in the Rio Negro basin would involve, in its initial stages, the acidic hydrolysis of  
394 clay minerals by the soil solution. This initial process may be favored by higher  
395 environmental humidity, consequently, the palaeoenvironmental conditions that led to the  
396 initial formation of the B spodic horizons were related to the time intervals of predominant  
397 humid climates during late Pleistocene (at ~40,000 cal BP and ~14,000 cal BP).

398           Some palaeoenvironmental studies have suggested similar humid intervals for the  
399 palaeoclimate in southeastern Brazil. Based on pollen analysis, Ledru et al. (1996), at Serra do  
400 Salitre, Minas Gerais State, ~ 1200 km west of VNR, suggested high moisture levels during  
401 the interval 40,000-27,000 BP (44,151-30,709 cal BP), with a maximum humidity at ~35,000  
402 BP (40,095-38,843 cal BP). In the same study, the authors inferred the gradual increase in the  
403 humidity after the late Glacial, during the interval 16,000 -11,000 BP (19,741-12,545 cal BP).  
404 Pessenda et al. (2009), at the Curucutu Nature Reserve, São Paulo State, ~1000 km south of  
405 VNR, used pollen analysis in a peatland and C isotopes in the soil organic matter, to infer the  
406 presence of a humid climate for the interval 28,000 - 15,000 BP (~31,500 - 18,000 cal BP),  
407 characterizing the expansion of Araucaria forest in the region, today located ~500 km to the  
408 south, at Paraná State. Veríssimo et al. (2012) studied a pollen record in the Serra do Caparaó,  
409 ~230 km from VNR, and inferred humid climate for the transition Pleistocene – Holocene  
410 (~11,500 cal BP). Based on  $\delta^{18}\text{O}$  of stalagmites from south and southeastern Brazil, Cruz Jr et  
411 al. (2005, 2006) suggested intervals of higher rainfall amounts around 45,000-40,000  
412 (~48,000 – 43,000 cal BP) and 20,000-14,000 BP (~ 24,000 – 17,000 cal BP) in the Bt2  
413 record, and around 47,000-37,000 (~ 50,000 – 40,000 cal BP) and 20,000-15,500 (~24,000 –  
414 18,500 cal BP) in the St8 record, caused by changes in the location and/or convective activity  
415 of the South American summer monsoon.

#### 416 **3.4. Micromorphology and genesis of soils**

417           The spodic horizons had similar micromorphological features (Table 4). Many areas  
418 observed in the thin sections had organic matter coatings completely filling the porous space,  
419 with a porphyric distribution pattern (Fig. 4c, 4e), a phenomenon already observed by Coelho  
420 et al. (2012) in spodic horizons formed in sandy materials from the coast of São Paulo state,  
421 Brazil. However, basic types of relative distribution such as chitonic, gefuric and enaulic can

422 be observed in the thin sections of the spodic B horizons (Fig. 4a). The organic matter in the  
423 spodic horizons, characterized by the advanced stage of transformation and absence of  
424 cellular structures or original forms of vegetable remnants, can be identified as monomorphic  
425 (De Coninck et al., 1974; Coelho et al., 2012).

426 In the studied horizons, there is a predominance of porosity cavity poly-concave, and  
427 the pores between the coarse grains of sub-rounded polycrystalline quartz (Fig. 4d) are filled  
428 with a fine organic matter of black tones in the central part and reddish at the extremities (Fig.  
429 4e). This change in coloration evolves with the formation of channels and micro fissures (Fig.  
430 4f), with subsequent separation of these constituents into smaller units, giving rise to complex  
431 microstructure with film bridges between grains and massive (Fig.4b).

432 In the study environment, the combination of factors such as excess moisture,  
433 temperature and high acidity, sediment of the Barreiras Formation and flat relief, contribute to  
434 the occurrence of the pedogenetic processes of ferrolysis (Dubroeuq and Volkoff, 1998;  
435 Moreau et al., 2006) and podzolisation (Lundström et al., 2000; Corrêa et al., 2008; Oliveira  
436 et al., 2010; Silva et al., 2013). In the area covered by forest vegetation (profile P6), one may  
437 infer that these processes are largely responsible for the transformation of sedimentary  
438 material from the Barreiras Formation, with destruction of clays by the ferrolysis process.  
439 This results in more sandy surface horizons followed by other clayey subsurface horizons and  
440 the formation of Acrisols.

441 In a lateral transformation sequence in Acrisols located in the higher parts of the study  
442 site, the ferrolysis at the top of the Bt horizon favored by the excess of moisture in this area of  
443 the profile, leads to the formation and thickening of the E horizon, at the expense of the Bt  
444 horizon (Mafra et al., 2002; Silva et al., 2013).

445 At a later stage, or simultaneously to the ferrolysis, the process of podzolisation takes  
446 place, in which organic compounds such as dissolved humic and fulvic acids, complex and

447 remove metals, mainly Fe and Al, from the superficial horizons (A, H), translocating and  
448 depositing them in the subsurface horizons and forming the spodic B (Mafra et al., 2002;  
449 Oliveira et al., 2010; Silva et al., 2013). These processes can be noted in the profiles P1, P2,  
450 P3, P4 and P5, located in the areas with grass vegetation, where there is a larger drainage  
451 impediment layer. Oliveira et al. (2010) have pointed out that the Podzols of the Barreiras  
452 Formation have a cemented spodic B horizon (Ortstein), which appears to have been formed  
453 due to the lateral transport of silica and aluminum, related to the destruction of clays from the  
454 duric horizons of Acrisols and Ferralsols, located in the higher portions of the landscape, as  
455 observed in the study area. In tropical conditions, which characterize our study, in sandy and  
456 poorly drained soil, the spodic B horizon contains plenty of organic complexes and Al, but  
457 little Fe oxides, which were reduced and removed by leaching.

458 The monomorphic predominance of the organic constituents evidences the  
459 mobilization, illuviation and precipitation of the organic matter in the genesis of the spodic  
460 horizon (De Coninck et al., 1974; De Coninck, 1980; Buurman et al., 2005; Coellho et al.,  
461 2012). The  $^{14}\text{C}$  ages indicate that the accumulation of organic material of  $\text{C}_3$  plants from the  
462 vegetation cover in B spodic horizons occurred since at least ~14,250 to 38,890 cal BP, in the  
463 profiles P4 and P1, respectively. These B horizons cause high-amplitude reflections in the  
464 GPR data, indicative of abrupt changes in wave energy, that are attributed to the formation of  
465 a cemented or indurated soil, with ortstein and duric horizon.

466 It is assumed that the genesis of the spodic horizons occurred in the past under  
467 accentuated hydromorphism (De Coninck, 1980; McKeague & Wang, 1980; Coellho et al.,  
468 2012). In Amazonian, the most waterlogged zones of the podzolized areas are the main source  
469 of dissolved organic matter, with an organic carbon accumulation rate in the Bh horizon of  
470  $0.54$  to  $3.17 \text{ g cm}^{-2} \text{ year}^{-1}$ , which requires a long time for organic matter stabilization, whose  
471  $^{14}\text{C}$  dating in the B spodic horizons ranged from 48,000 to 450,000 years BP (Doupoux, et al.,

472 2017). On the other hand, changes in the precipitation pattern, with greater frequency of dry  
473 periods, resulting in less frequent waterlogging, decrease carbon flux to the Bh horizon  
474 (Sierra et al., 2013), promoting instability and degradation of organic matter mainly at the top  
475 of the B spodic horizon (Coelho et al., 2012). This hypothesis is supported by the fact that the  
476 differentiated coloration of organic matter in the voids is associated with different degrees of  
477 decomposition, indicating differences in the chemical constituents of this organic material  
478 (Buurman et al., 2005; Bardy et al., 2008). In an evolutionary stage of decomposition of the  
479 organic matter, the microfissures are formed, which evolve originating the voids space inter-  
480 grains of the cavity poly-concave type, initiating the process of destruction of the top B spodic  
481 horizon.

#### 482 **4. Conclusions**

483 The ground penetrating radar images showed that development of soil horizons occurs  
484 directly over the weathered bedrock of the Barreiras Formation. The horizons in the top of  
485 radargrams were differentiated by changes in the internal geometry of the reflectors and are  
486 consistent with the findings of the soil pedons. The data also showed that spodic horizons in  
487 transects 1 and 2 have variable thicknesses, which possibly correlate with podzolisation  
488 processes, which reflect the lateral changes of the depth and degree of weathering of the  
489 Barreiras Formation. The combination of a near-surface water table, humidity and excessive  
490 acidity and sandy nature of the sediment of the Barreiras Formation, have favoured the  
491 processes of ferrolysis and podzolisation. The destruction of clays and eluviation of organic  
492 matter complexed with aluminum provided the genesis of Acrisols and Podzols, respectively.  
493 The filling of the voids space by organic constituents evidences the process of illuviation of  
494 the organic matter, responsible for the genesis of the B spodic horizons. The accumulation of  
495 organic compounds in the B spodic horizons of the P1 and P4 profiles originated from C<sub>3</sub>  
496 plants, suggests the dominance of humid climate in the region since at least 38,890 cal BP.

497 **Acknowledgments**

498 To FUNDECT; to the CNPq/CAPES for the financial support through projects:  
499 “Casadinho” process 620029/20080 and “Casadinho/Procad” process 552377/2011-2; to  
500 CNPq (470210/2012-5, 302711/2013-9) and FAPESP (2007/03615-5, 2010/18091-4 and  
501 2011/00995-7) for the financial support for the field trips and analyses.

502 **References**

- 503 Afshar, A.F., Ayoubi, S., Castrignanò, A., Quarto, R., Ardekani, M. R. M., 2017. Using  
504 ground-penetrating radar to explore the cemented soil horizon in an arid region in Iran.  
505 *Near Surface Geophysics*, 15, 103-110.
- 506 Anderson, H.A., Berrow, M.L., Farmer, V.C., Hepburn, A., Russel, J.D., Walker A.D., 1982.  
507 A reassessment of podzol formation processes. *Journal of Soil Science*, 33(1), 125-136.
- 508 Bardy, M., Fritsch, E., Derenne, S. Allard, T., do Nascimento, N.R., Bueno, G.T. (2008).  
509 Micromorphology and spectroscopic characteristics of organic matter in waterlogged  
510 podzols of the upper Amazon basin. *Catena*, 145, 222-230.
- 511 Bockheim, J.G., Hartemink, A. E., 2013. Soils with fragipans in the USA. *Catena* 104, 233-  
512 242.
- 513 Boski, T., Angulo, R.J., Souza, M.C., Barboza, E.G., Knicker, H., González-Pérez, J.A.,  
514 González-Vila, F.J., 2015. Progradation rates of coastal barrier sands estimated from the  
515 <sup>14</sup>C age of soil organic matter. *J. Quart. Sci.* 30, 9–18.
- 516 Bullock, P., Fedoroff, N., Jongerius, A., Stoops, G., Tursina, T., 1985. *Handbook for Soil*  
517 *Thin Section Description*. Waine Research Publications, Wolverhampton (152 pp).
- 518 Burgoa, B., Mansell, R.S., Sawka, G.J., Nkedi-Kizza, P., Capece, J., Campbell, K., 1991.  
519 Spatial variability of depth to Bh horizon in Florida Haplaquods using ground-penetrating  
520 radar. *Soil and Crop Science Society of Florida Proceedings*, 50, 125–130.

- 521 Buso Junior, A.A., Pessenda, L.C.R., De Oliveira, P.E., Giannini, P.C.F., Cohen, M.C.L.,  
522 Volkmer-Ribeiro, C., Oliveira, S.M.B., Rossetti, D.F., Lorente, F.L., Borotti Filho, M.A.,  
523 Schiavo, J.A., Bendassolli, J.A., França, M.C., Guimarães, J.T.F., Siqueira, G.S., 2013a.  
524 Late Pleistocene and Holocene vegetation, climate dynamics, and Amazonian taxa in the  
525 Atlantic Forest, Linhares, SE Brazil. *Radiocarbon* 55 (2-3), 1747-1762.
- 526 Buso Junior, A.A., Pessenda, L.C.R., Mayle, F.E., Lorente, F.L., Volkmer-Ribeiro, C.,  
527 Schiavo, J.A.,, Pereira, M.G., Bendassolli, J.A., Macario, K.C.D., Siqueira, G.S. 2019.  
528 Paleovegetation and paleoclimate dynamics during the last 7000 years in the Atlantic  
529 Forest of Southeastern Brazil based on palynology of a waterlogged sandy soil. *Review*  
530 *of Palaeobotany and Palynology* 264, 1–10.
- 531 Buurman, P.; Jongmans, A.G. 2005. Podzolisation and soil organic matter dynamics.  
532 *Geoderma* 125, 71-83.
- 533 Buurman, P.; van Bergen, P.F.; Jongmans, A.G.; Meijer, E.L.; Duran, B., Van Lagen, B.  
534 (2005). Spatial and temporal variation in podzol organic matter studied by pyrolysis-gas  
535 chromatography/mass spectrometry and micromorphology. *Eur. J. Soil Sci.*, 56:253-270.
- 536 Buurman, P., 1984. Podzols. Van Nostrand Reinhold Soil Science Series New York.  
537 (450 pp).
- 538 Buurman, P., Vidal-Torrado, P., Martins, V.M., 2013. The podzol hydrosequence of Itaguapé  
539 (Sao Paulo, Brazil). 1. Geomorphology and interpretation of profile morphology. *Soil*  
540 *Sci. Soc. Am. J.* 77, 1294–1306.
- 541 Calegari, M.R., Madella, M., Brustolin, L.T., Pessenda, L.C.R., Buso Júnior, A.A.,  
542 Francisquini, M.I., Bendassolli, J.A., Vidal-Torrado, P., 2017. Potential of soil phytoliths,  
543 organic matter and carbon isotopes for small-scale differentiation of tropical rainforest  
544 vegetation: A pilot study from the campos nativos of the Atlantic Forest in Espírito Santo  
545 State (Brazil). *Quaternary International*, 437, 156-164.



- 546 Carvalho, V.S., Ribeiro, M.R., Souza Júnior, V.S., Brilhante, S.A., 2013. Caracterização de  
547 Espodossolos dos Estados da Paraíba e do Pernambuco, Nordeste do Brasil. *Revista*  
548 *Brasileira de Ciência do Solo*, 37, 1454-1463.
- 549 Coelho, M.R., Martins, V.M., Vidal-Torrado, P., Souza, C.R.G., Perez, X.L.O., Vázquez,  
550 F.M., 2010 b. Relação solo-relevo-substrato geológico nas restingas da planície costeira  
551 do Estado de São Paulo. *Revista Brasileira de Ciência do Solo*, 34(2), 833-846.
- 552 Coelho, M.R., Vidal-Torrado, P., Perez, X.L.O., Martins, V.M., Vázquez, F.M., 2010c.  
553 Fracionamento do Al por técnicas de dissoluções seletivas em Espodossolos da planície  
554 costeira do estado de São Paulo. *Revista Brasileira de Ciência do Solo*, 34(2), 1081-1092.
- 555 Coelho, M. R., Martins, V.M., Pérez, X.L.O., Vázquez, F.M., Gomes, F.H., Cooper, M.,  
556 Vidal-Torrado, P., 2012. Micromorfologia de horizontes Espódicos nas restingas do  
557 Estado de São Paulo. *Revista Brasileira de Ciência do Solo*, 36, 1380-1394.
- 558 Corrêa, M.M., Ker, J.C., Barrón, V., Torrent, J., Fontes, M.P.F., Curi, N., 2008. Propriedades  
559 cristalográficas de caulinitas de solos do ambiente tabuleiros costeiros, Amazônia e  
560 Recôncavo Baiano. *Revista Brasileira de Ciência do Solo*, 32 (3), 1857-1872.
- 561 Cruz Jr, F.W., Burns, S.J., Karmann, I., Sharp, W.D., Vuille, M., Cardoso, A.O., Ferrari, J.A.,  
562 Dias, P.L.S., Viana Jr, O., 2005. Insolation-driven changes in atmospheric circulation  
563 over the past 116,000 years in subtropical Brazil. *Nature* 434, 63-66.
- 564 Cruz Jr, F.W., Burns, S.J., Karmann, I., Sharp, W.D., Vuille, M., 2006. Reconstruction of  
565 regional atmospheric circulation features during the late Pleistocene in subtropical Brazil  
566 from oxygen isotope composition of speleothems. *Earth and Planetary Science Letters*  
567 248, 495-507.

- 568 Dantas, J.S., Marques Júnior, J., Martins Filho, M.V., Resende, J.M.A., Camargo, L.A., &  
569 Barbosa, R.S. (2014). Gênese de solos coesos do leste maranhense: relação solo-  
570 paisagem. *Revista Brasileira de Ciência do Solo*, 38(3), 1039-1050.
- 571 de Castro, S.S., Cooper, M., Santos, M.C., Vidal-Torrado, P., de Lima, J.M., 2003.  
572 Micromorfologia do solo: bases e aplicações. In: Curi, N., Marques, J.J., Guilherme,  
573 L.R.G., Lopes, A.S., Alvarez Venegas, V.H. (Eds.), *Tópicos em ciência do solo*. Vol. 3.  
574 Sociedade Brasileira de Ciência do Solo, Viçosa, MG, pp. 107–164.
- 575 De Coninck, F. 1980. Major mechanisms in formation of spodic horizons. *Geoderma*, 24:101-  
576 126.
- 577 De Coninck, F.; Righi, D.; Maucorps, J., Robin, A.M. 1974. Origin and micromorphology  
578 nomenclature of organic matter in sandy spodosols. In: Rutheford, G.K., ed. *Soil*  
579 *microscopy*. Ontario, Limestone Press. p.263-273.
- 580 Dias, H.C.T., Schaefer, C.E.G.R., Fernandes Filho, E.I., Oliveira, A.P., Michel, R.F.M.,  
581 Lemos, J.B., 2003. Caracterização de solos Altimontanos em dois transectos no Parque  
582 Estadual do Ibitipoca (MG). *Revista Brasileira de Ciência do Solo*, 27(2), 469-481.
- 583 Doolittle, J.A., Collins, M.E., 1995. Use of soil information to determine application of  
584 ground-penetrating radar. *Journal of Applied Geophysics* 33, 101–108.
- 585 Doolittle, J.A., Butnor, J.R., 2009. Soils, peatlands and biomonitoring. In: *Ground Penetrating*  
586 *Radar: Theory and Applications* (ed H.M. Jol), p. 179. Amsterdam, Netherlands:  
587 Elsevier.
- 588 Doolittle, J., Daigle, J., Kelly, J., Tuttle, W., 2005. Using GPR to characterize plinthite and  
589 ironstone layers in Ultisols. *Soil Survey Horizons* 46(4), 179–184.
- 590 Doupoux. C., Merdy, P., Montes, R.C., Nunan, N., Melfi, A.J., Pereira, O.J.R., Lucas, Y.,  
591 2017. Modelling the genesis of equatorial podzols: age and implications for carbon  
592 fluxes. *Biogeosciences*, 14 (1), 2429–2440.

- 593 Dubroeuq, D., Volkoff, B., 1998. From Oxisols to Spodosols and Histosols: evolution of the  
594 soil mantles in the rio Negro basin (Amazonia). *Catena*, 32(1), 245-280.
- 595 Farmer, V.C., Russel, J.D., Smith, B.F.L., 1983. Extraction of inorganic forms of translocated  
596 Al, Fe and Si from a Podzol Bs horizon. *European Journal of Soil Science*, 34(3), 571-  
597 576.
- 598 Gomes, F.H., Vidal-Torrado, P., Macías-Vazquez, F., Gherardi, B., Otero, X.L., 2007. Solos  
599 sob vegetação de restinga na Ilha do Cardoso-SP: I- Caracterização e classificação.  
600 *Revista Brasileira de Ciência do Solo*, 31 (4), 1563-1580.
- 601 Hogg, A.G., Hua, Q., Blackwell, P.G., Niu, M., Buck, C.E., Guilderson, T.P., Heaton, T.J.,  
602 Palmer, J.G., Reimer, P.J., Reimer, R.W., Turney, C.S.M., Zimmerman, S.R.H., 2013.  
603 SHCal13 Southern Hemisphere calibration, 0-50,000 years cal BP. *Radiocarbon* 55 (4),  
604 1889-1903.
- 605 Horbe, A.M.C., Horbe, M.A. & Suguio, K. 2004. Tropical Spodosols in northeastern  
606 Amazonas State, Brazil. *Geoderma*, 119, 55–68.
- 607 IUSS Working Group WRB, 2015. World reference base for soil resources 2014, update  
608 2015. International soil classification system for naming soils and creating legends for  
609 soil maps. *World Soil Resources Reports No. 106*. FAO, Rome (1-192 pp.).
- 610 Kaczorek, D., Sommer, M., Andruschkewitsch, L., Oktaba, L., Czerwinski, Z., Stahr, K.,  
611 2004. A comparative micromorphological and chemical study of “Raseneisenstein”(bog  
612 iron ore) and “Orstein”. *Geoderma* 121, 83–94.
- 613 Kämpf, N., Curi, N. Formação e evolução do solo (Pedogênese). In: Ker, J.C., Curi, N.,  
614 Schaefer, C.E.G.R., Vidal Torrado, P., 2012. *Pedologia: Fundamentos*. (1ª ed.). Viçosa:  
615 SBCS, p.207-302.

- 616 Ledru, M-P., Braga, P.I.S., Soubiès, F., Fournier, M., Martin, L., Suguio, K., Turcq, B., 1996.  
617 The last 50,000 years in the Neotropics (Southern Brazil): evolution of vegetation and  
618 climate. *Palaeogeography, Palaeoclimatology, Palaeoecology* 123, 239-257.
- 619 Lima Neto, J.A., Ribeiro, M.R., Corrêa, M.M., Souza Júnior, V.S., Lima, J.F.W.F., Ferreira,  
620 R.F.A.L., 2009. Caracterização e gênese do caráter coeso em Latossolos Amarelos e  
621 Argissolos dos Tabuleiros Costeiros do Estado de Alagoas. *Revista Brasileira de Ciência*  
622 *do Solo*, 33(4), 1001-1011.
- 623 Lopes-Mazzetto, J.M., Schellekens, J. Pablo Vidal-Torrado, P., Buurman, P. 2018. Impact of  
624 drainage and soil hydrology on sources and degradation of organic matter in tropical  
625 coastal podzols. *Geoderma*, 330, 79-90.
- 626 Lundstrom, U.S., van Breemen, N., Bain, D.C., van Hees, P.A.W., Giesler, R., Gustafsson,  
627 J.P., Ilvesniemi, H., Karlton, E., Melkerud, P.A., Olsson, M., Riise, G., Wahlberg, O.,  
628 Bergelin, A., Bishop, K., Finlay, R., Jongmans, A.G., Magnusson, T., Mannerkoski, H.,  
629 Nordgren, A., Nyberg, L., Starr, M., Tau Srand, L., 2000a. Advances in understanding  
630 the podzolization process resulting from a multidisciplinary study of three coniferous  
631 forest soils in the Nordic Countries. *Geoderma* 94, 335–353.
- 632
- 633 Macario, K.D., Gomes, P.R.S., Anjos, R.M., Carvalho, C., Linares, R., Alves, E.Q., Oliveira,  
634 F.M., Castro, M.D., Chanca, I.S., Silveira, M.F.M., Pessenda, L.C.R., Moraes, L.M.B.,  
635 Campos, T.B., Cherkinsky, A, 2013. The Brazilian AMS radiocarbon laboratory (LAC-  
636 UFF) and the intercomparison of results with CENA and UGAMS. *Radiocarbon* 55 (2-3),  
637 325-330.
- 638 Mafra, A.L., Miklós, A.A.W., Volkoff, B., & Melfi, A.J. (2002). Pedogênese numa seqüência  
639 Latossolo-Espodosolo na região do alto rio negro, Amazonas. *Revista Brasileira de*  
640 *Ciência do Solo*, 26(2), 381-394.

- 641 Macko, S.A., Estep, M.L.F. (1984). Microbial alteration of stable nitrogen and carbon  
642 isotopic compositions of organic matter. *Organic Geochemistry*, 6:787–90.
- 643 Martin, L., Suguio, K., Flexor, J.M., 1993. As flutuações do nível do mar durante o  
644 Quaternário superior e a evolução de “deltas” brasileiros. *Boletim IG-USP* 15,  
645 1e186.
- 646 Martinez, P., Lopes-Mazzeto, J.M., Buurman, P., Giannini, P.C.F., Schellekens, J., Vidal-  
647 Torrado, P., 2018. Geomorphological control on podzolisation – An example from a  
648 tropical barrier island. *Geomorphology* 309, 89–97.
- 649 McKeague, J.A., Wang, C. (1980). Micromorphology and energy dispersive analysis of  
650 orstein horizons of podzolic soils from New Brunswick and Nova Scotia, Canada. *Can. J.*  
651 *Soil Sci.*, 60:9-21, 1980.
- 652 McKeague, J.A., Day, J.H., 1966. Dithionite-and oxalate-extractable Fe and Al as aids in  
653 differentiating various classes of soils. *Canadian Journal Soil Science*, 1(1), 13-22.
- 654 Mehra, O.P., Jackson, M.L. 1960. Iron oxide removal from soils and clays by a dithionite-  
655 citrate system buffered with sodium bicarbonate. *Clays and Clay Minerals*, 7(2), 317-27.
- 656 Mendonça, B.A.F., Fernandes Filho, E.I., Schaefer, C.E.G.R., Simas, F.N.B., de Paula, M.D.  
657 2015. Os solos das Campinaranas na Amazônia brasileira: ecossistemas arenícolas  
658 oligotróficos. *Ciência Florestal*, Santa Maria, 25 (4), 827-839.
- 659 Ministério do Meio Ambiente, 2000. Avaliação e Ações Prioritárias para a Conservação da  
660 Biodiversidade da Mata Atlântica e Campos Sulinos. MMA/SBF, Brasília, p. 40.

- 661 Montes, C.R., Lucas<sup>2</sup>, O. J. R. Pereira<sup>1</sup>, R. Achard<sup>2,\*</sup>, M. Grimaldi<sup>2</sup>, and A. J. Melfi. Deep  
662 plant-derived carbon storage in Amazonian podzols. 2011. *Biogeosciences*, 8, 113–120.
- 663 Moreau, A.M.S.S., Ker, J.C., Costa, L.M., Gomes, F.H., 2006. Caracterização de solos de  
664 duas topossequências em Tabuleiros Costeiros do sul da Bahia. *Revista Brasileira de*  
665 *Ciência do Solo*, 30(4), 1007-1019.
- 666 Mokma, D.L., Schaetzl, R.J., Doolittle, J.A., Johnson, E.P., 1990. Groundpenetrating radar  
667 study of ortstein continuity in some Michigan Haplaquods. *Soil Sci Soc Am J* 54:936–  
668 938.
- 669 Oliveira, A.P., Ker, J.C., Silva, I.R., Fontes, M.P.F., de Oliveira, A.P., Neves, A.T.G.R.,  
670 2010. Spodosols pedogenesis under Barreiras formation and sandbank environments in  
671 the south of Bahia. *Revista Brasileira de Ciência do Solo*, 34(3), 847-860.
- 672 Perrin, R.M.S., Willis, E.H., Hodge, C.A.H., 1964. Dating of humus podzols by residual  
673 radiocarbon activity. *Nature* 202(4928), 165-166.
- 674 Pessenda, L.C.R., Valencia, E.P.E., Camargo, P.B., Telles, E.C.C., Martinelli, L.A., Cerri,  
675 C.C., Aravena, R., Rozanskj, K., 1996. Natural radiocarbon measurements in Brazilian  
676 soils developed on basic rocks. *Radiocarbon* 38(2), 203-208.
- 677 Pessenda, L.C.R., Buso Junior, A.A., Cohen, M.C.L., Calegari, M.R., Schiavo, J.A., França,  
678 M., Lorente, F.L., Giannini, P.C.F., Oliveira, P.E., Rossetti, D.F., Siqueira, G.S.,  
679 Francisquini, M.I., Volkmer-Ribeiro, C., Bendassoli, J.A., Madella, M., Osterrieth, M.,  
680 Cechet, F.A., Felipe, P.L.L., Brustolin, L.T., Rasbold, G.G., Monteiro, M.R., 2015.  
681 Estudos interdisciplinares da dinâmica da vegetação e marinha e inferências climáticas  
682 milenares e atuais na costa Norte do Espírito Santo. *Ciência & Ambiente*, 49(1), 181-206.
- 683 Pessenda L.C.R., De Oliveira, P.E., Mofatto, M., Medeiros, V.B., Garcia, R.J.F., Aravena, R.,  
684 Bendassoli, J.A., Leite, A.Z., Saad, A.R., Etchebehere, M.L., 2009. The evolution of a

- 685 tropical rainforest/grassland mosaic in southeastern Brazil since 28,000 14C yr BP based  
686 on carbon isotopes and pollen records. *Quaternary Research*, 71, 437- 452.
- 687 Santos, H.G., Jacomine, P.K.T., Anjos, L.H.C., Oliveira, V.A., Lumberras, J.F., Coelho,  
688 M.R., Almeida, J.A., Araújo Filho, J. C., Oliveira, J. B., Cunha, T.J.F. 2018. Sistema  
689 Brasileiro de Classificação de Solos. 5<sup>a</sup> ed. revisada e ampliada. Brasília, DF: Embrapa,  
690 531p.
- 691 Santos, R.D.; Santos, H.G.; Ker, J.C., Anjos, L.H.C.; Shimizu, S.H. 2015. Manual de  
692 descrição e coleta de solo no campo. 7.ed. Viçosa, MG, Sociedade Brasileira de Ciência  
693 do Solo/Embrapa Solos, 100p.
- 694 Saporetto-Junior, A.W., Schaefer, C.E.R.; Souza, A.L., Soares, M.P., Araújo, D.S.D., Meira-  
695 Neto, J.A.A., 2012. Influence of soil physical properties on plants of the mussununga  
696 ecosystem, Brazil. *Folia Geobotanica* 47, 29-39.
- 697 Sauer, D., Sponagel, H., Sommer, M., Giani, L., Jahn, R., Stahr, K., 2007. Podzol: soil of the  
698 year 2007. A review on its genesis, occurrence, and functions. *J. Plant Nutr. Soil Sci.* 170  
699 (5):581–597. <https://doi.org/10.1002/jpln.200700135>.
- 700 Schiavo, J.A., Dias Neto, A.H., Pereira, M.G., Rosset, J.S., Secretti, M.L., Pessenda, L.C.,  
701 2012. Characterization and classification of soils in the Taquari river basin - Pantanal  
702 Region, State of Mato Grosso do Sul, Brazil. *Revista Brasileira de Ciência do Solo*,  
703 36(3), 697-707.
- 704 Schwartz, D., 1988. Some podzols on Bateke sands and their origins, People's Republic of  
705 Congo. *Geoderma* 43, 229-247.
- 706 Sierra, C.A., Jiménez, E.M., Reu, B., Peñuela, M.C., Thuille, A., Quesada, C.A., 2013. Low  
707 vertical transfer rates of carbono inferred from radiocarbon analysis in na Amazon  
708 Podzol. *Biogeosciences*, 10 (1), 3455–3464.

- 709 Silva, E.A., Gomes, J.B.V., Araújo Filho, J.C., Silva, C.A., de Carvalho, S.A, Curi, N., 2013.  
710 Podzolização em solos de áreas de depressão de topo dos tabuleiros costeiros do Nordeste  
711 Brasileiro. *Revista Brasileira de Ciência do Solo*, 37(1), 11-24.
- 712 Soil Survey Staff. *Keys to soil taxonomy*. 12th. ed. Washington, DC: USDA, Natural  
713 Resources Conservation Service; 2014.
- 714 Stoops, G., 2003. *Guidelines for Analysis and Description of Soil and Regolith Thin Sections*.  
715 Soil Science Society of America, Madison, Wisconsin.
- 716 Stuiver, M., Reimer, P.J., 1993. Extended 14C database and revised CALIB 3.0 14C  
717 calibration program. *Radiocarbon* 35 (1), 215-230.
- 718 Teixeira, P.C.; Donagemma, G.K.; Fontana, A.; Teixeira, W.G. 2017. *Manual de métodos de*  
719 *análise de solo*. Rio de Janeiro, 3ª ed. Revisada e ampliada – Brasília, DF: Embrapa,  
720 573p.
- 721 Ucha, J.M., Vilas Boas, G.S, Hadlich, G.M. 2010. O uso do radar de penetração no solo na  
722 investigação dos processos de transformação pedogeomorfológica. *Revista Brasileira de*  
723 *Geomorfologia*, 11 (1), 85-96.
- 724 Van Breemen, N.V., Buurman, P., 1998. *Soil formation*. Dordrecht, Kluwer.
- 725 Veríssimo, N., Safford, H.DF., Behling, H., 2012. Holocene vegetation and fire history of the  
726 Serra do Caparaó, SE Brazil. *The Holocene* 22(11), 1243-1250.
- 727 Yeomans, J.C., Bremner, J.M., 1988. A rapid and precise method for routine determination of  
728 organic carbon in soils. *Communications Soil Science Plant Analysis*, 19 (4), 1467-1476.
- 729
- 730
- 731
- 732
- 733



734

735

736

737

738

739

740

741

742

743

744

745

746

747

748

749

750

751

752

753

754

755

756

757

758

759

760

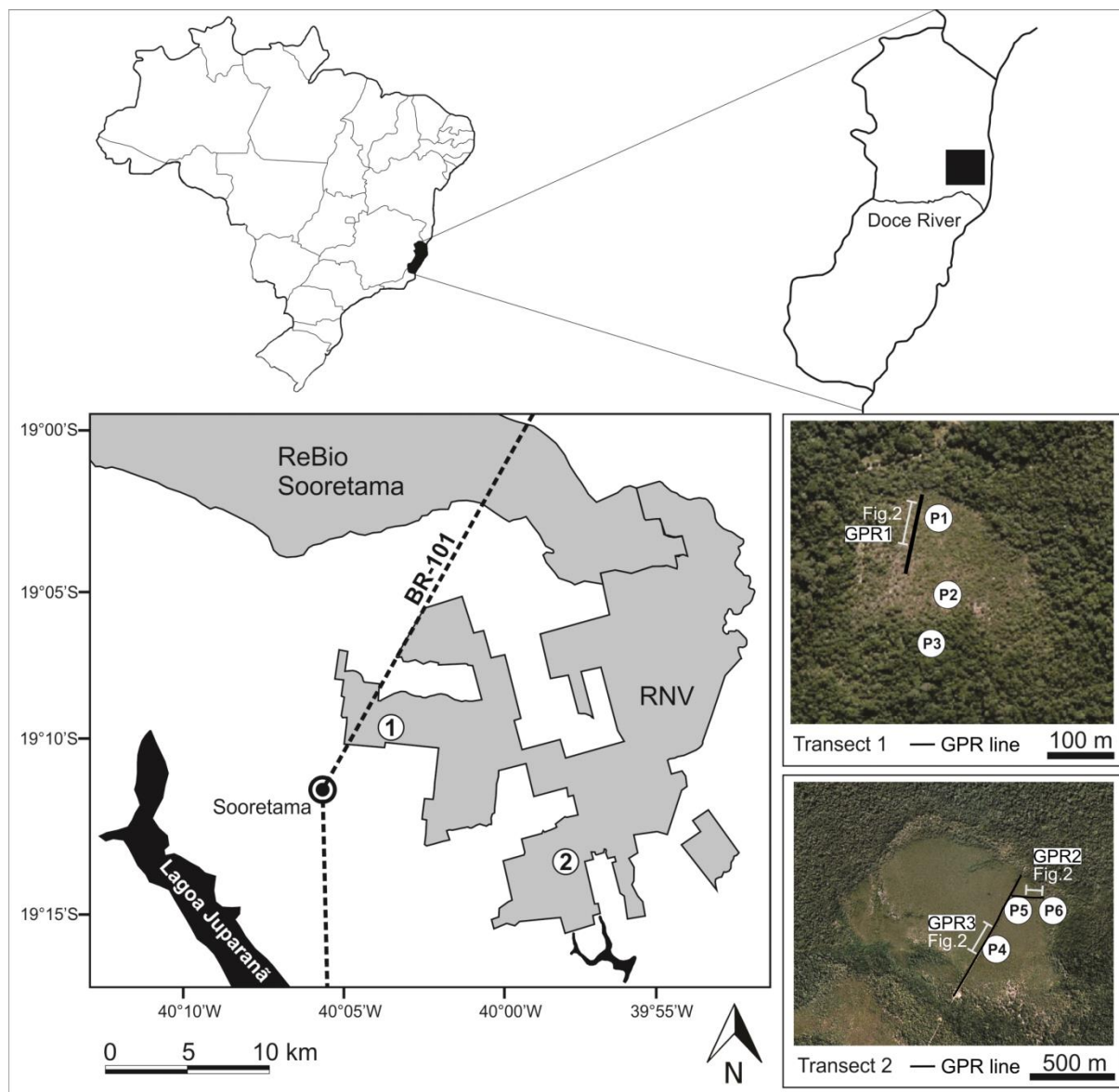
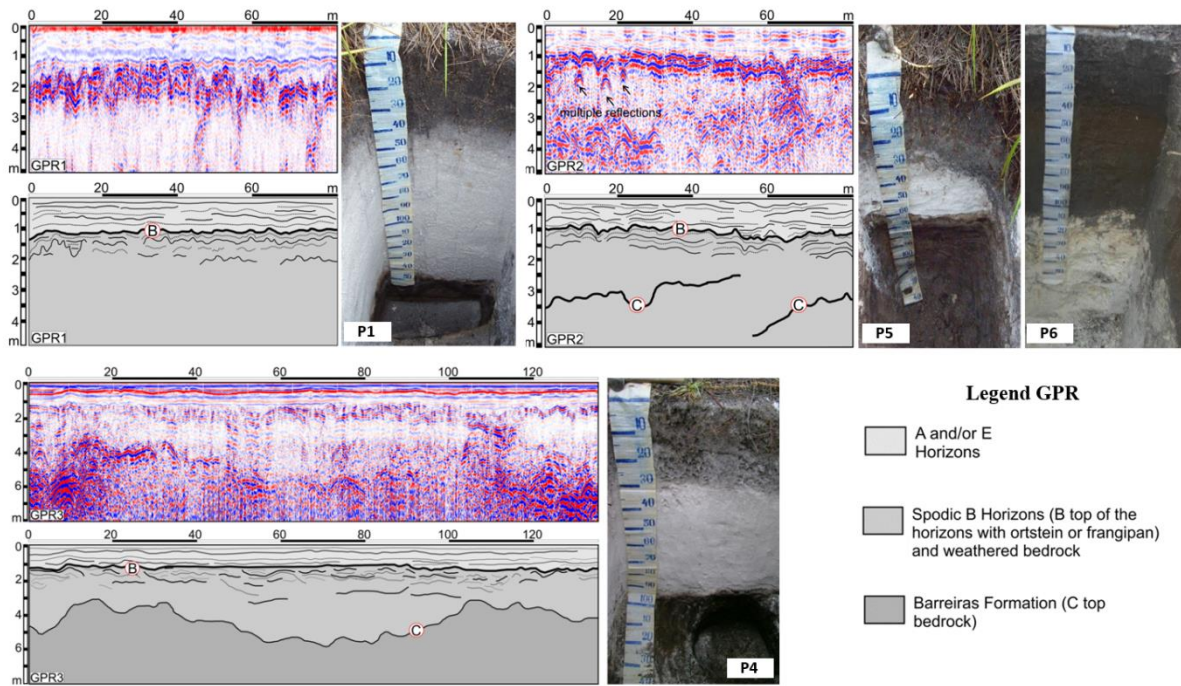


**Figure 1.** Study area map showing sampling locations and Ground penetrating radar (GPR) activities in the forest grassland ecotone areas in the northeastern Espirito Santo State, Brazil. Transect 1 (profiles 1, 2 and 3) and Transect 2 (profiles 4, 5 and 6).

761



762

763

764 **Figure 2.** Ground penetrating radar (GPR) data and interpretation of the radargram with the  
 765 different soils horizons and deposits of the Barreira Formation identified in the profile.

766

767

768

769

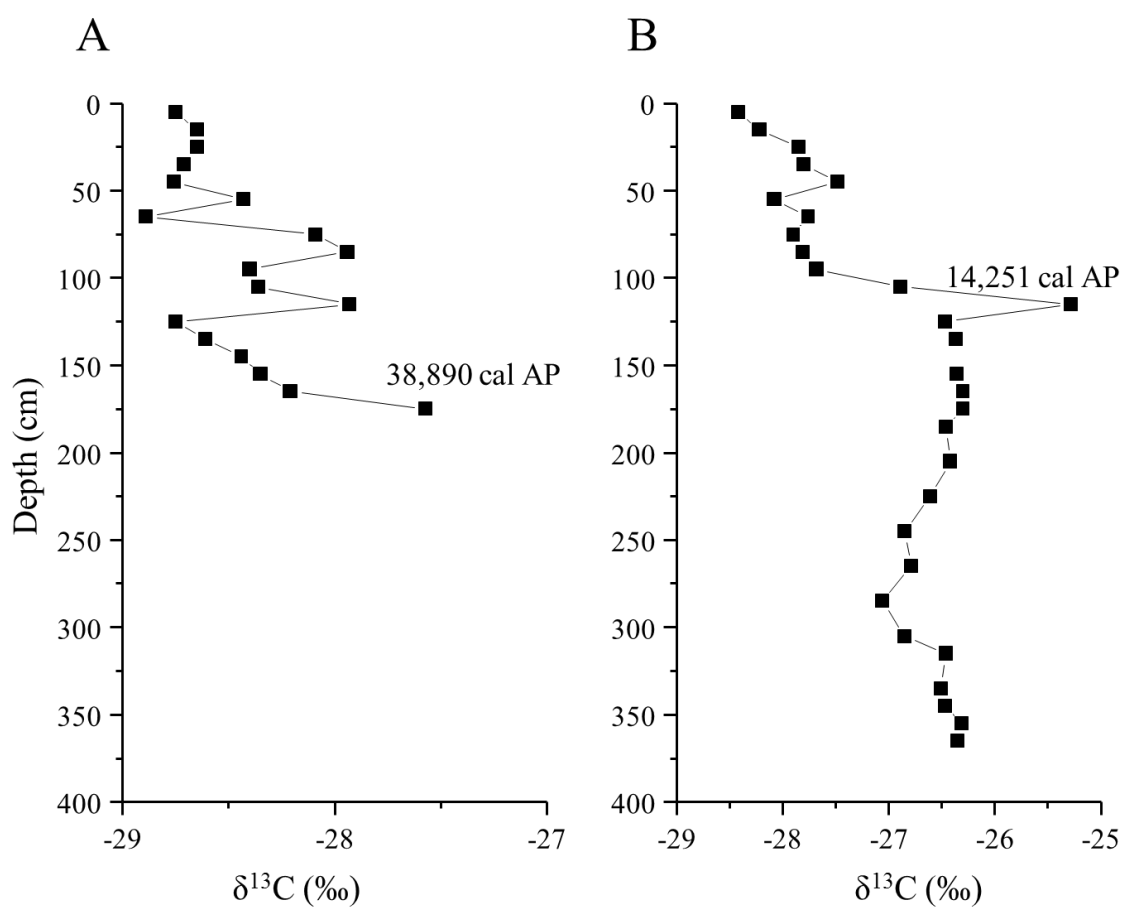


**Figure 3.** Variation of  $\delta^{13}\text{C}$  (‰) and  $^{14}\text{C}$  ages in profiles P1 (A) and P4 (B) of Podzols in the northeastern Espírito Santo State, Brazil.

770

771

772

773

774

775

776

777

778

779

780

781

782

783



784

785

786

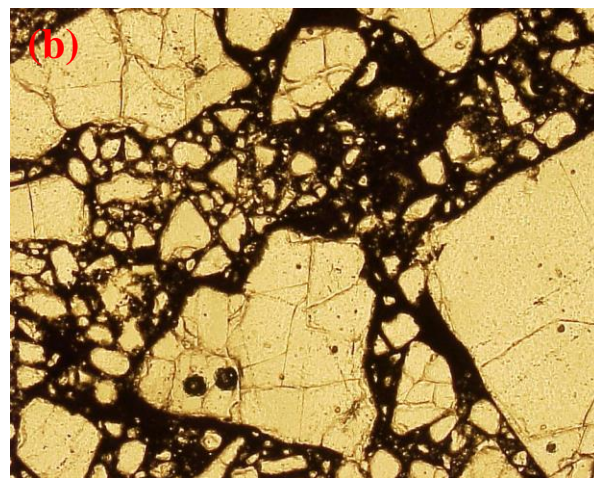
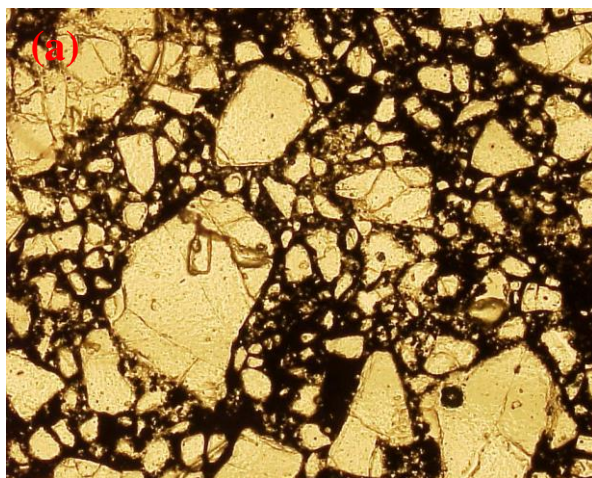
787

788

789

790

791



792

793

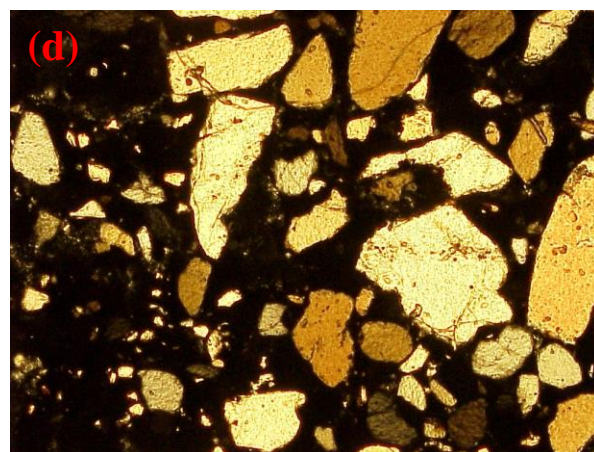
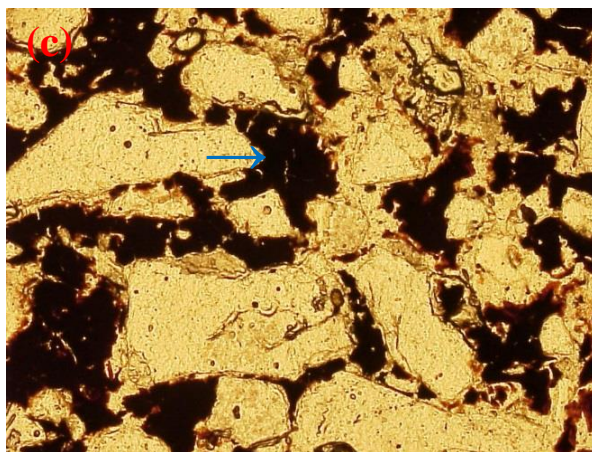
794

795

796

797

798



799

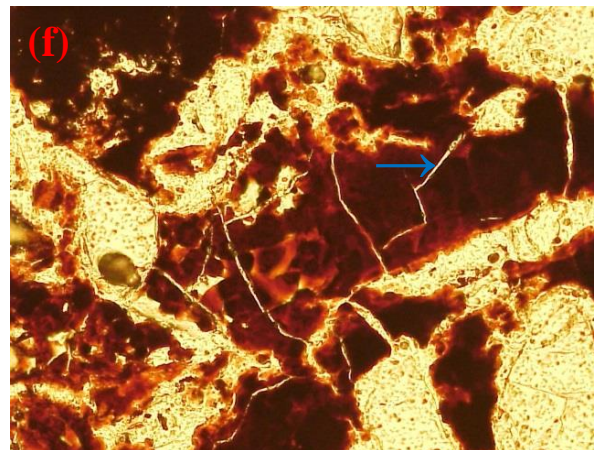
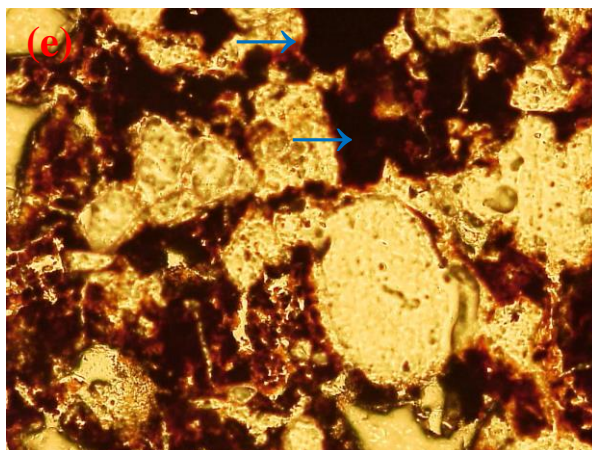
800

801

802

803

804



805

**Figure 4.** Photomicrographs in which can be observed: Horizon Bhm profile P2: (a) relative distribution chitonic-gefuric-porphyrin; (b) complex pellicular microstructure with bridges and massive. Horizon Bh2 profile P5: (c) monomorphic organic matter completely filling the porosity (relative distribution  $g/f_{2\mu m}$  porphyric); (d) coarse material, with quartz grains and porosity cavity poly-concave; (e) fine organic material filling the voids space, with dark coloration in the central part and reddish at the extremities; (f) presence of microfissures and dissolution of fine organic material.

813

814

815 **Table 1.** Morphological and granulomeric attributes of soils developed in the forest grassland  
816 ecotone areas in the northeastern Espirito Santo State, Brazil.

Horizon	Depth m	Munsell color		Structure <sup>1</sup>	Consistence			Transition <sup>5</sup>	Sand	Clay	Silt	Texture class
		moist	dry		dry <sup>2</sup>	moist <sup>3</sup>	wet <sup>4</sup>					
<b>Transect 1 - P1 – grassland</b>												
A1	0-0.18	10YR 3/1	10YR 4/1	we, sm/me, gr	sf	fb	np, ss	pc	982	4	14	Sand
A2	0.18-0.36	10YR 4/1	10YR 5/1	sg	l	ls	np, ns	pa	970	4	26	Sand
E	0.36-1.43	10YR 8/1	10YR 8/1	sg	l	ls	np, ns	pa	945	2	53	Sand
Bhm1	1.43-1.49	10YR 3/1	10YR 5/2	massive	eh	ef	np, ns	pa	771	9	220	Loamy sand
Bhx1	1.49-1.60	10YR 3/1	10YR 4/2	mo, sm, ab	h	fb	np, ns	pa	683	23	294	Sandy loam
Bhx2	1.60-1.74 <sup>+</sup>	10YR 3/2	10YR 5/1	mo, sm, ab	h	fb	np, ns	-	668	29	303	Sandy loam
<b>P2- shrubland</b>												
A1	0-0.15	10YR 3/1	10YR 4/1	we, sm/me, gr	sf	fb	np, ns	pc	845	10	145	Loamy sand
A2	0.15-0.25	10YR 4/1	10YR 5/1	sg	l	ls	np, ns	pa	922	7	71	Sand
E	0.25-0.61	10YR 8/1	10YR 8/1	sg	l	ls	np, ns	pa	919	71	10	Sand
Bhm	0.61-0.74	10YR 2/1	10YR 3/1	massive	h	fb	np, ns	pc	723	24	253	Loamy sand
Bx1	0.74-0.98	10YR 4/2	10YR 5/3	massive	vh	fb	np, ns	pc	692	31	277	Sandy loam
Bx2	0.98-1.40 <sup>+</sup>	10YR 5/3	10YR 6/3	massive	vh	fb	np, ns	-	757	157	86	Loamy sand
<b>P3 - woodland</b>												
H	0-0.12	2,5Y 2,5/1	2,5Y 3/1	mo,sm,gr	l	ls	np, ns	pc	885	77	38	Sand
A1	0.12-0.26	2,5Y 2,5/1	2,5Y 2,5/1	sg	l	ls	np, ns	pc	912	72	16	Sand
A2	0.26-0.40	2,5Y 4/1	2,5Y 5/1	sg	l	ls	np, ns	pc	940	53	7	Sand
E1	0.40-0.57	2,5Y 5/2	2,5Y 7/1	sg	l	ls	np, ns	pa	943	40	17	Sand
E2	0.57-1.34	2,5Y 7/1	2,5Y 8/1	sg	l	ls	np, ns	pa	918	56	26	Sand
Bhm	1.34-1.41	2,5Y 5/3	2,5Y 6/3	massive	eh	f	np, ns	pc	801	75	124	Loamy sand
Bhx1	1.41-1.49	10YR 4/2	2,5Y 5/2	massive	eh	ef	np, ns	pc	716	145	139	Loamy sand
Bhx2	1.49-1.69 <sup>+</sup>	2,5Y 3/1	2,5 3/1	massive	h	vf	np, ns	-	657	293	50	Sandy clay loam
<b>Transect 2 – P4 – grassland</b>												
A1	0-0.16	10YR 4/1	10YR 5/1	sg	l	ls	np, ns	pc	981	4	15	Sand
A2	0.16-0.22	10YR 4/1	10YR 5/1	sg	l	ls	np, ns	pc	970	4	26	Sand
E	0.22-0.91	10YR 8/1	10YR 8/1	sg	l	ls	np, ns	oa	945	2	53	Sand
Bhm1	0.91-0.93	10YR 4/1	10YR 5/2	massive	eh	vf	np, ss	pa	751	9	240	Loamy sand
Bhm2	0.93-1.11	10YR 3/1	10YR 3/2	massive	h	f	np, ss	pa	872	16	112	Sand
Bh	1.11-1.28 <sup>+</sup>	2,5Y 2,5/1	2,5Y 2,5/1	mo, sm, Bs	sf	fb	np, ns	-	610	36	354	Sandy loam
<b>P5 – shrubland</b>												
A1	0-0.11	10YR 2/1	10YR 3/1	mo, me/l, gr	sf	fb	np, ns	pc	892	10	98	Sand
A2	0.11-0.34	10YR 3/1	10YR 4/1	sg	l	ls	np, ns	oc	924	8	68	Sand
E	0.34-0.60	10YR 7/1	10YR 8/1	sg	l	ls	np, ns	pa	916	8	76	Sand
Bhm	0.60-0.70	10YR 5/2	10YR 5/2	massive	eh	vf	np, ns	pc	711	12	277	Loamy sand
Bh1	0.70-0.87	10YR 2/1	10YR 3/1	mo, sm, ab	l	ls	np, ns	pc	545	45	410	Sandy loam
Bh2	0.87-1.15	10YR 3/2	10YR 4/2	mo, sm, ab	h	fb	np, ss	pc	748	23	229	Loamy sand
Bh3	1.15-1.24 <sup>+</sup>	10YR 3/2	10YR 4/2	mo, sm, ab	h	fb	np, ss	-	610	36	354	Sandy loam
<b>P6 – woodland</b>												
A1	0-0.15	10YR 2/2	10YR 3/1	mo, sm, gr	sh	f	sp, ss	pc	774	183	43	Sandy loam
A2	0.15-0.34	10YR 2/1	10YR 3/2	mo, sm, gr	sh	f	sp, ss	pc	741	214	45	Sandy clay loam
A3	0.34-0.58	2,5Y 3/3	2,5Y 4/3	mo, sm, gr	h	f	np, ns	pc	708	262	30	Sandy clay loam
A4	0.58-0.73	2,5Y 3/2	2,5Y 5/3	mo, sm, sab	sh	fb	sp, ns	pc	732	246	22	Sandy clay loam
A5	0.73-1.00	2,5Y 3/2	2,5Y4/2	mo, sm, sab	sh	fb	sp, ns	pc	733	255	12	Sandy clay loam
Btg1	1.00-1.29	2,5Y 8/3	2,5Y 8/2	mo, sm, sab	h	f	p, s	pa	191	430	379	Clay
Btg2	1.29-1.50	2,5Y 8/3	2,5Y8/2	mo, sm, sab	h	f	p, s	pc	168	487	345	Clay
Btg3	1.50-1.82 <sup>+</sup>	2,5Y 8/3	2,5Y 8/2	mo, sm, sab	h	f	p, s	-	284	366	350	Clay loam

817 <sup>1</sup>Structure: degree of development: (we: weak, mo: moderate), size (sm: small, me: medium, l: large), shape (gr:  
818 granular, sg: simple grains, ab: angular blocks, sab: subangular blocks ). <sup>2</sup>Dry consistence: (sf: soft, l: loose, eh:  
819 extremely hard, h: hard, vh: very hard, sh: slightly hard). <sup>3</sup>Moist consistence: (fb: friable, ls: loose, ef: extremely  
820 firm, f: firm, vf: very friable). <sup>4</sup>Wet consistence: (np: not plastic, p: plastic; sp: slightly plastic; ss: slightly sticky,  
821 ns: not sticky). <sup>5</sup>Transition: (pc: plain and clear, pa: plain and abrupt, oa: ondulation and abrupt, oc: ondulation  
822 and clear).

823

824

825

826 **Table 2.** Chemical attributes of soils developed in the forest grassland ecotone areas in the  
 827 northeastern Espirito Santo State, Brazil.

Horizon	Depth	TOC	pH		P	K <sup>+</sup>	Na <sup>+</sup>	Ca <sup>2+</sup>	Mg <sup>2+</sup>	H+Al	Al <sup>3+</sup>	SB	T	m	V
			Water	KCl											
	m	g kg <sup>-1</sup>			mg kg <sup>-1</sup>	cmolc kg <sup>-1</sup>					%				
<b>Transect 1 - P1 – grassland</b>															
A1	0-0.18	14.5	4.4	2.6	7	0	0.09	0.9	0.3	11.3	1.7	1.3	12.6	14	10
A2	0.18-0.36	16.7	4.4	2.7	12	0	0.01	1.0	0.2	5.6	1.3	1.2	6.8	19	18
E	0.36-1.43	3.7	5.3	4.3	1	0	0.01	0.3	0.1	0.4	0.1	0.4	0.8	12	51
Bhm1	1.43-1.49	19.0	4.0	2.8	2	0	0.01	0.2	0.2	17.8	4.5	0.4	18.2	25	2
Bhx1	1.49-1.60	26.5	4.1	3.4	33	0	0.01	0.3	0.1	33.2	4.5	0.4	33.6	13	1
Bhx2	1.60-1.74 <sup>+</sup>	30.5	4.2	3.6	28	0	0.01	0.3	0.1	15.0	3.1	0.4	15.4	20	3
<b>P2- shrubland</b>															
A1	0-0.15	14.5	4.3	2.4	13	0	0.23	2.1	1.0	26.4	2.1	3.3	29.7	7	11
A2	0.15-0.25	5.2	4.3	2.6	18	0	0.02	0.7	0.2	6.9	1.2	0.9	7.8	15	12
E	0.25-0.61	5.0	5.1	3.7	0	0	0.01	0.3	0.1	0.2	0.1	0.4	0.6	16	67
Bhm	0.61-0.74	27.5	4.0	3.0	8	0	0.06	0.4	0.1	35.9	8.6	0.6	36.5	24	2
Bx1	0.74-0.98	8.2	4.1	3.6	26	0	0.38	0.1	0.1	15.1	5.1	0.6	15.7	33	4
Bx2	0.98-1.40 <sup>+</sup>	9.2	4.3	3.7	117	0	0.37	0.0	0.1	14.3	3.2	0.5	14.8	22	3
<b>P3- woodland</b>															
H	0-0.12	92.3	4.1	2.8	21	0	0.39	0.4	2.9	22.6	4.7	3.3	25.9	41	13
A1	0.12-0.26	45.5	4.5	2.9	9	0	0	0.3	1.0	10.7	2.2	1.3	12.0	37	11
A2	0.26-0.40	21.3	4.5	3.2	9	0	0	0.4	0.2	7.6	1.5	0.6	8.2	29	7
E1	0.40-0.57	9.6	5.8	3.6	5	0	0	0.2	0.1	4.8	0.5	0.3	5.1	38	6
E2	0.57-1.34	7.0	6.0	4.6	3	0	0	0.3	0.2	4.9	0.3	0.5	5.4	63	9
Bhm	1.34-1.41	15.8	6.1	4.0	4	0	0	0.2	0.8	5.4	0.6	1.0	6.4	63	16
Bhx1	1.41-1.49	15.2	6.2	3.8	6	0	0	0.1	0.7	10.0	3.3	0.8	10.8	20	7
Bhx2	1.49-1.69 <sup>+</sup>	61.0	6.1	4.0	23	0	0	0.3	0.2	19.6	6.7	0.5	20.1	7	2
<b>Transect 2 – P4 – grassland</b>															
A1	0-0.16	8.0	4.2	2.7	5	0	0.01	0.5	0.2	5.5	0.9	0.7	6.2	14	11
A2	0.16-0.22	2.3	4.5	2.9	5	0	0.01	0.8	0.3	3.3	0.6	1.1	4.4	14	25
E	0.22-0.91	1.8	5.2	4.4	0	0	0.02	0.5	0.2	1.2	0.2	0.7	1.9	10	37
Bhm1	0.91-0.93	7.2	4.2	2.8	0	0	0.01	0.3	0.1	10.8	1.5	0.4	11.2	13	4
Bhm2	0.93-1.11	35.2	3.8	2.6	0	0	0.01	0.5	0.3	56.2	7.6	0.8	57.0	13	1
Bh	1.11-1.28 <sup>+</sup>	33.9	3.9	2.8	2	0	0.01	1.0	0.4	49.6	5.8	1.4	51.0	11	3
<b>P5 – shrubland</b>															
A1	0-0.11	6.3	3.9	2.6	11	0	0.16	0.9	0.3	16.2	2.5	1.4	17.6	14	8
A2	0.11-0.34	9.3	4.1	2.7	6	0	0.02	0.3	0.2	6.5	1.5	0.5	7.0	21	7
E	0.34-0.60	2.0	4.7	4.0	0	0	0.02	0.5	0.2	0.2	0.2	0.7	0.9	22	78
Bhm	0.60-0.70	22.5	4.2	3.2	1	0	0.02	0.2	0.1	10.6	2.9	0.3	10.9	27	3
Bh1	0.70-0.87	14.5	4.4	3.3	14	0	0.01	0.2	0.1	30.3	5.9	0.3	30.6	19	1
Bh2	0.87-1.15	18.2	4.4	3.8	29	0	0.01	0.1	0.1	12.4	2.5	0.2	12.6	20	2
Bh3	1.15-1.24 <sup>+</sup>	25.5	4.3	3.7	13	0	0.01	0.3	0.1	11.9	3.1	0.4	12.3	25	3
<b>P6 – woodland</b>															
A1	0-0.15	58.5	4.5	3.6	13	0	0.14	0.3	0.1	12.1	2.5	0.4	12.5	14	3
A2	0.15-0.34	38.1	4.7	3.8	11	0	0.32	0.4	0.3	15.0	2.4	0.7	15.7	23	4
A3	0.34-0.58	58.8	4.9	4.1	8	0	0.12	0.3	0.1	24.0	3.0	0.4	24.8	12	2
A4	0.58-0.73	48.7	5.0	4.2	6	0	0.12	0.3	0.1	18.2	1.9	0.4	18.6	17	2
A5	0.73-1.00	37.0	5.0	4.3	6	0	0.14	0.3	0.1	14.5	1.8	0.4	14.9	18	3
Btg1	1.00-1.29	16.4	5.0	4.1	4	0	0.08	0.3	0.2	8.0	1.7	0.5	8.5	23	6
Btg2	1.29-1.50	17.2	5.0	4.2	4	0	0.00	0.3	0.2	6.6	2.0	0.5	7.1	20	7
Btg3	1.50-1.82 <sup>+</sup>	21.1	4.9	4.1	5	0	0.06	0.3	0.1	6.0	1.5	0.4	6.4	21	6

828 TOC: total organic carbono (method of Yeomans e Bremner); pH em água e KCl (1:2,5); P, K e Na:  
 829 extracted by Mehlich-1; Ca, Mg e Al: extracted by KCl 1 mol L<sup>-1</sup>; H+Al: extracted by calcium acetate  
 830 0,5 mol L<sup>-1</sup> pH 7,0; SB: bases of sum; m: saturation by aluminum; V: saturation by bases.



832 **Table 3.** Fe e Al extracted by oxalate (Ox) and dithionite-citrate-bicarbonate (DCB) and the  
 833 ratio of these metals of soils developed in the forest grassland ecotone areas in the  
 834 northeastern Espirito Santo State, Brazil.

Horizon	Depth m	Oxalate			DCB			Al <sub>ox</sub> /Al <sub>DCB</sub>	Fe <sub>ox</sub> /Fe <sub>DCB</sub>
		Al	Fe	Al/Fe	Al	Fe	Al/Fe		
—g kg <sup>-1</sup> —									
<b>Transect 1 - P1 – grassland</b>									
A1	0-0.18	0.02	0.02	0.68	0.00	0.48	0.00	0.00	0.05
A2	0.18-0.36	0.00	0.01	0.00	0.00	0.45	0.00	0.00	0.02
E	0.36-1.43	0.00	0.00	0.00	0.00	0.58	0.00	0.00	0.01
Bhm1	1.43-1.49	0.90	0.01	87.94	0.62	0.52	1.21	1.44	0.02
Bhx1	1.49-1.60	3.38	0.01	413.47	4.06	0.52	7.77	0.83	0.02
Bhx2	1.60-1.74 <sup>+</sup>	2.59	0.04	58.59	1.71	0.47	3.68	1.51	0.09
<b>P2- shrubland</b>									
A1	0-0.15	0.16	0.04	4.04	0.04	0.95	0.04	4.07	0.04
A2	0.15-0.25	0.03	0.02	1.48	0.00	0.87	0.00	0.00	0.02
E	0.25-0.61	0.00	0.01	0.00	0.00	0.83	0.00	0.00	0.01
Bhm	0.61-0.74	3.78	0.05	69.51	4.29	0.90	4.78	0.88	0.06
Bx1	0.74-0.98	2.89	0.02	117.26	1.91	0.73	2.61	1.51	0.03
Bx2	0.98-1.40 <sup>+</sup>	5.26	0.03	167.68	3.49	0.88	3.96	1.51	0.04
<b>P3- woodland</b>									
H	0-0.12	0.02	0.04	0.43	0.27	0.47	0.58	0.07	0.09
A1	0.12-0.26	0.02	0.01	1.44	0.23	0.53	0.45	0.09	0.03
A2	0.26-0.40	0.01	0.01	0.95	0.18	0.47	0.38	0.05	0.02
E1	0.40-0.57	0.00	0.00	0.41	0.13	0.39	0.35	0.01	0.01
E2	0.57-1.34	0.00	0.00	0.25	0.29	0.49	0.59	0.00	0.01
Bhm	1.34-1.41	0.05	0.04	1.09	0.56	0.56	1.00	0.08	0.08
Bhx1	1.41-1.49	0.99	0.05	17.99	1.14	0.45	2.55	0.87	0.12
Bhx2	1.49-1.69 <sup>+</sup>	6.24	0.19	33.33	3.85	0.40	9.55	1.62	0.46
<b>Transect 2 – P4 – grassland</b>									
A1	0-0.16	0.00	0.02	0.00	0.00	0.42	0.00	0.00	0.05
A2	0.16-0.22	0.00	0.01	0.00	0.00	0.56	0.00	0.00	0.02
E	0.22-0.91	0.00	0.00	0.00	0.00	0.55	0.00	0.00	0.01
Bhm1	0.91-0.93	0.49	0.03	15.88	0.28	0.46	0.61	1.76	0.07
Bhm2	0.93-1.11	3.48	0.01	241.19	3.48	0.51	6.88	1.00	0.03
Bh	1.11-1.28 <sup>+</sup>	3.28	0.01	247.33	3.65	0.61	6.03	0.90	0.02
<b>P5 – shrubland</b>									
A1	0-0.11	0.08	0.10	0.82	0.00	0.68	0.00	0.00	0.15
A2	0.11-0.34	0.05	0.04	1.17	0.00	0.43	0.00	0.00	0.10
E	0.34-0.60	0.00	0.01	0.00	0.00	0.41	0.00	0.00	0.01
Bhm	0.60-0.70	0.83	0.03	23.81	0.91	0.61	1.50	0.91	0.06
Bh1	0.70-0.87	4.85	0.04	129.02	5.70	0.50	11.43	0.85	0.08
Bh2	0.87-1.15	2.22	0.02	136.38	2.37	0.74	3.19	0.93	0.02
Bh3	1.15-1.24 <sup>+</sup>	1.77	0.02	76.26	1.51	0.67	2.26	1.17	0.03
<b>P6 – woodland</b>									
A1	0-0.15	1.15	0.22	5.15	1.50	0.66	2.27	0.77	0.34
A2	0.15-0.34	2.40	0.15	16.49	1.90	0.48	3.97	1.26	0.30
A3	0.34-0.58	18.23	0.62	29.44	15.48	0.70	21.97	1.18	0.88
A4	0.58-0.73	11.25	0.34	33.34	11.02	0.67	16.37	1.02	0.50
A5	0.73-1.00	8.57	0.14	61.95	7.12	0.45	15.68	1.20	0.30
Btg1	1.00-1.29	5.13	0.57	9.05	3.44	0.84	4.09	1.49	0.68
Btg2	1.29-1.50	3.56	0.42	8.39	2.47	0.78	3.16	1.44	0.54
Btg3	1.50-1.82 <sup>+</sup>	3.34	0.31	10.88	2.39	0.65	3.67	1.40	0.47

835

836

837

838

839 **Table 4.** Main micromorphological characteristics of the subsurface horizons of soils  
 840 developed in the forest grassland ecotone areas in the northeastern Espirito Santo State,  
 841 Brazil.

	Transect 1. Profile P2- grasses. Bhm - Bx1. 0.61-0.98 m.	Transect 2. Profile P5- grasses. Bh2. 0.87-1.15 m.
Matrix	Coarse material: 65% Fine material: 20% Porosity: 15%	Coarse material: 50% Fine material: 35% Porosity: 15%
Relative distribution	Complex: chitonic-gefuric-porphyric.	Complex: porphyric-enaulic.
Coarse material	Composed of polycrystalline quartz grains, sub-rounded, subangular, smooth/wavy, sub sphere and poorly selected. Frequency: dominant (60-70%).	Composed of polycrystalline quartz grains, sub-rounded, subangular, smooth/wavy, sub sphere and poorly selected. Frequency: dominant (60-70%).
Fine material	Predominantly organic matter and clay	Clay, iron oxide and mainly organic matter.
Pores	Porosity cavity, poly-concave, with irregular cavities, channels, fissures and microfissures. Presence of some stacking pores	Porosity cavity, poly-concave, stacking. Some channels and microfissures in the fine material.
Microstructure	Complex: Film (organic matter and clay) with bridges and massive.	Complex: polyhedral microgranular aggregates with presence of coalesced zones forming a dense mass
Birefringent fabric	Undifferentiated	Undifferentiated
Pedological features	Grains covered by cutans of organic material.	Grains covered by cutans of organic material.

842

843

844

845